



UNIVERSIDAD NACIONAL DE COLOMBIA

Surface global irradiance assessed by three different methods

Pingyun Zheng

鄭平允

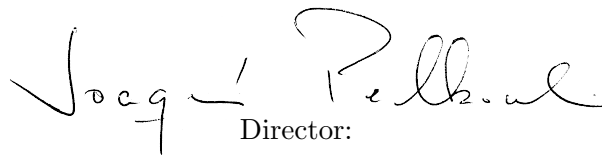
Universidad Nacional de Colombia
Facultad de Ciencias, Departamento de Geociencias
Bogotá, Colombia
2018

Surface global irradiance assessed by three different methods

Pingyun Zheng

鄭平允

Tesis presentada como requisito parcial para optar al título de:
Magíster en Ciencias - Meteorología



Director:

Ph.D., Meteorólogo, Joaquín Pelkowski Goebel

Línea de Investigación:
Radiación atmosférica, especialmente irradiancia en superficie

Universidad Nacional de Colombia
Facultad de Ciencias, Departamento de Geociencias
Bogotá, Colombia

2018

*In memory of my parents
For all the love you gave*

After three years you both passed away, I arrived at this antipodean continent, taking up studies once again, and I know you would be gratified that I am learning what I am truly interested in and enjoying my life with inner peace.

Acknowledgements

Foremost, I would like to thank my supervisor Dr. Joaquín Pelkowski, it is hard to describe how privileged I have been to study with him. Let alone his erudition and rigorous attitude towards science, he also has an amazing personality. He supervised me with great patience, and always encouraged and respected my ideas, which made my two years study a very enjoyable process. I am pleased to know him as a friend and mentor.

I was lucky that I met my wonderful schoolmates. Among them, a big thank to Edwin Torres. We have become best friends inside and outside campus ever since the incredible coincidence of meeting for the first time at the same table for our entrance exam. He has helped me go through countless problems I encountered. Also thanks to Diego Quintero, for many cheerful lunches during long days of study, and two outstanding rock concerts. I am grateful to my fellows Alfonso Ladino, Dario Poveda, Hugo Rico, Danys Ortiz, for many helps you gave and letting me see the Colombians' warm hearts.

My thanks also go out to my friends in China. I would specially like to thank Jiajing Liu, many chats with her about the direction of my career along with all kinds of subjects. I would like to thank all the supports from Zun Wei, Chen Qiu, Qiliang Wu, Yongmao Lin, Feiyu Yang, and many more. Thanks so much to my big family in China for always caring about me.

I am grateful to the Muñoz family, who kindly accommodated me for one year, treating me as a family member. Special thanks to Andrew Dagleish whom I met in the same family, we have had some fabulous hikes, and many interesting talks about the movies since we are both cinephiles.

I would like to express my gratitude to the university—who gave me a chance to enjoy the study and the science again, special thanks to Professor Emel Vega, one of the most friendly and warmhearted professors I have seen; Professor Daniel Hernandez, I always asked him all kinds of questions, related or unrelated to my study topic, also thanks for his superb string quartet concerts (he is a great violist!); Karina Garzón, former secretary of the department, helped me out of a lot of formalities and procedures.

Finally, I would like to express my gratitude to Colombia—giving me a precious experience, and all the friends I have known in this country.

Abstract

Three methods will be used to evaluate the surface global irradiance: radiative transfer theory, empirical regression, and artificial neural networks (ANN). Radiative transfer is the fundamental theory that describes the propagation of radiation through a medium; empirical regression predicts surface global irradiance in simple parameterizations; artificial neural network, as an artificial intelligence technique, can also be tried to assess the surface global irradiance. These three approaches are studied in the present work. Data from the station “EL IDEAM” were used in the modeling experiments built upon these approaches to evaluate the daily transparency, also known as clearness index. We found out that the optimal inputs for artificial neural networks are extraterrestrial irradiance, surface relative humidity, and a pollution index based on particulate matter of sizes less than $10\mu m$ (PM_{10}). Surface relative humidity was suggested in a regression trial under meteorological conditions of “EL IDEAM”. By means of the programming code DISORT for the solution of the radiative transfer equation, daily irradiance characteristics were analyzed, and a hybrid model was created. Our results showed that artificial neural network produces higher scores than the other methods, though advantages and drawbacks are also discussed and compared.

keywords: surface global irradiance, clearness index, linear regression, artificial neural network, radiative transfer, DISORT.

Contents

Acknowledgements	vii
Abstract	ix
1. Introduction	1
2. Radiative transfer	3
2.1. Fundamentals and prerequisites	3
2.2. An overview of the main approaches for solving the RTE	7
2.2.1. Discrete ordinates	7
2.2.2. Successive orders of scattering	8
2.2.3. Invariant imbedding	9
2.2.4. Adding and doubling	9
2.2.5. Integral equation	9
2.2.6. Feautrier method	9
2.2.7. Spherical harmonics	10
2.2.8. Monte Carlo	10
2.2.9. Comparison among approaches	10
2.3. A deeper look into discrete ordinates	11
2.3.1. Isotropic scattering	11
2.3.2. Two-stream approximation	13
2.3.3. Inhomogeneous atmosphere	17
2.3.4. Scaling of phase function	18
2.4. Application and minimal layering of atmosphere	19
3. Statistics-driven approaches: empirical and neural network	22
3.1. Why do we need them?	22
3.2. Empirical approaches	23
3.2.1. Ångström–Prescott-type models	23
3.2.2. Models involving other meteorological variables	24
3.2.3. Direct irradiance models	25
3.3. Artificial intelligence technique	26

4. Data	28
4.1. On the upper boundary condition	28
4.2. Global irradiance data	30
4.2.1. The station	30
4.2.2. From hourly measurements to daily values.	31
4.3. Variables for predicting global irradiance	33
4.4. Summary and size of dataset	35
5. Experiments and results	37
5.1. Design of experiments	37
5.2. Empirical regression	39
5.3. Artificial neural network	41
5.3.1. Architecture of neural networks	41
5.3.2. Input variables and performances	46
5.4. Radiative transfer method	50
5.4.1. Feature of irradiance in tri-layered model	50
5.4.2. Prediction by DISORT	52
6. Conclusions	55
Appendix A. Approaches for solving the RTE	58
A.1. Successive orders of scattering	58
A.2. Invariant imbedding	59
A.3. Adding and doubling	60
Appendix B. Data validation methodology	62
B.1. Validation procedure	62
B.1.1. Irradiance data	62
B.1.2. Other variables	64
B.2. Testing and preparing the dataset	64
Bibliography	65

1. Introduction

Solar energy is the predominant driving force responsible for most activities on Earth, the form of which is electromagnetic radiation. After a little more than 8 minutes of an undisturbed journey, a solar beam intercepted by the Earth will undergo some changes. The intensity at the top of the Earth's atmosphere is fairly stable, by virtue of the steady output of the Sun's burning rate and the small eccentricity of the Earth's orbit. Our concern here is the energy amount that will be able to reach the surface, an amount known as the global irradiance, whose prediction is complicated due to the interference of the Earth's ever-changing atmosphere.

The general purpose of this thesis is assessment of solar irradiance by indirect measurements.

For that purpose the theory of radiative transfer, originally developed by astrophysicists, is available in an ever increasing wealth of treatises and at a highly sophisticated mathematical level. Radiative transfer is the fundamental theory that describes how radiation passing materials is modified. It has been codified since the important treatise by Chandrasekhar (1950). The radiative transfer equation (RTE), which is the master equation of the whole transfer theory, is an integro-differential equation that challenges both mathematical methods of solution and computational programming of its discrete form. Many techniques have been developed to seek at least approximate solutions. The complexity rises when the physical process of radiative transfer involves many factors, most of which hinge on radiative properties of materials along the path and thermodynamic conditions along it. That makes parameterization or simplifications unavoidable in actual applications. Models of our atmosphere can be simplified based on data available.

One of the most notable and long-tested “parameterizations” is the empirical method of Ångström and Prescott (Ångström 1924; Prescott 1940) called Ångström–Prescott regression. Its simplest depends on only one variable—sunshine duration. It is widely used in areas where direct measurement equipment is not available. Besides Ångström–Prescott regression, there are countless numbers of other regression models that try to explore relationships between global solar irradiance and other atmospheric variables.

It was not until the last decades that artificial neural networks (ANN) attracted attention among application-minded researchers, especially since computing power has become so widely available. ANN belongs to the artificial intelligence technique called *machine learning*, by which a computer learns patterns of existing data, to predict new data through

“training”. Since application to global irradiance, many authors draw the conclusion that ANN can predict results that are superior to traditional regression methods (Elminir *et al.* 2007; Jiang 2008).

The particular purposes of the present work then, are to explore the three approaches: radiative transfer, empirical regression and neural network, by studying their theories and characteristics, then by doing numerical experiments with recorded data.

Following this introductory Chapter 1, Chapter 2 is devoted to the theory of radiative transfer, while empirical methods and neural network technique are discussed in Chapter 3. Chapter 4 deals with the data, while Chapter 5 builds models based on different approaches with an analysis of the prediction results, beginning with empirical regression, continued neural network, and then proceeding to consider the radiative transfer approach. Finally Chapter 6 discusses the conclusions. Validation procedures for the dataset is left to Appendix B.

2. Radiative transfer

2.1. Fundamentals and prerequisites

If monochromatic intensity of radiation is denoted by I_ν , defined by a vector in the direction of propagation flux per unit of area and solid angle, the monochromatic net flux (or irradiance) in direction \mathbf{n} (perpendicular to a unit area) can be written as:

$$Q_\nu(\mathbf{n}) = \int_{4\pi} I_\nu(\boldsymbol{\Omega}) \cdot \mathbf{n} d\boldsymbol{\Omega}, \quad (2.1)$$

where $d\boldsymbol{\Omega}$ is an infinitesimal solid angle. In spherical polar coordinates, with zenith angle θ and azimuthal angle ϕ , the integral over solid angles becomes $\int_{4\pi} d\boldsymbol{\Omega} = \int_0^{2\pi} \int_0^\pi \sin\theta d\theta d\phi$. Letting \mathbf{n} be the direction for which $\theta = 0$, we find $I_\nu(\boldsymbol{\Omega}) \cdot \mathbf{n} = I_\nu(\theta, \phi) \cos\theta$, so that, Eq. (2.1) becomes

$$Q_\nu(\mathbf{n}_{\theta=0}) = \int_0^{2\pi} \int_0^\pi I_\nu(\theta, \phi) \cos\theta \sin\theta d\theta d\phi. \quad (2.2)$$

The net energy crossing an area ΔA (perpendicular to \mathbf{n}) in a certain interval of time Δt and a frequency band of $\Delta\nu$ is found by multiple integrations:

$$E(\mathbf{n}_{\theta=0}) = \int_{\Delta t} \int_{\Delta\nu} \int_{\Delta A} \int_0^{2\pi} \int_0^\pi I_\nu(\theta, \phi) \cos\theta \sin\theta d\theta d\phi dA d\nu dt. \quad (2.3)$$

Light passing through some interactive material, is subject to the processes of absorption, scattering and emission. The fundamental radiative transfer equation describing the interactions can be expressed in terms of extinction of the intensity and sources of radiation, S_ν :

$$-\frac{dI_\nu(s, \theta, \phi)}{\kappa_\nu \rho ds} = I_\nu(s, \theta, \phi) - S_\nu(s, \theta, \phi). \quad (2.4)$$

ρ refers to the density of the interactive material of mass extinction coefficient denoted as κ_ν . Eq. (2.4) describes how radiation dI_ν varies along with infinitesimal path ds in the material.

Our goal is to estimate or calculate irradiance or flux density, and for that we need to make several simplifications, among which we mention the following ones:

1. Radiation is assumed to be unpolarized, which means that, only the first component of the Stokes vector, the intensity I , is taken into account.

2. The Earth's atmosphere will be regarded as a horizontally plane-parallel medium, that is, we ignore the curvature of the Earth, on account of the fact that the atmosphere is very thin compared to the radius of the Earth.
3. Solar radiation can be regarded as parallel or as a collimated beam at the Sun-Earth distance, in view of the Earth's disk area intercepting the Sun's radiation.
4. Our atmosphere is grey in a first and crude approximation, i.e., it is taken to be a wavelength-indifferent medium.
5. All processes involving long-wave radiation, namely, radiation whose wavelength is by definition longer than $4\mu m$, are not of concern, because its contribution to solar energy received at surface is negligible.
6. Azimuthal independence in scattering processes. Azimuthal dependency can be accounted for by carrying out a Fourier decomposition.

Based on the second simplification, if we define

$$\tau_\nu = \int_s^\infty \beta_e ds' = \int_s^\infty \kappa_\nu \rho ds' \quad (2.5)$$

as optical depth in a plane-parallel atmosphere, and calling $\beta_e = \kappa_\nu \rho$ the extinction coefficient, then Eq. (2.4) can be written in the form

$$\mu \frac{dI_\nu(\tau_\nu, \mu, \phi)}{d\tau_\nu} = I_\nu(\tau_\nu, \mu, \phi) - S_\nu(\tau_\nu, \mu, \phi) \quad (2.6)$$

as new independent angular variable with $\mu \equiv \cos \theta$. Note that $\mu < 0$ indicates downward directions of radiations, as in the case of the solar beam in our atmosphere. Furthermore, the fourth simplification implies that, the subscript “ ν ” can be suppressed henceforward. The general solution of the inhomogeneous first-order differential equation (2.6) is:

$$I(\tau, \mu, \phi) = I(\tau_0, \mu, \phi) e^{-\frac{\tau_0 - \tau}{\mu}} - \frac{1}{\mu} \int_{\tau_0}^{\tau} S(\tau', \mu, \phi) e^{-\frac{\tau' - \tau}{\mu}} d\tau'. \quad (2.7)$$

Following the third simplification, the solar radiation outside the atmosphere could be viewed as being restrained to a single angle with cosine $-\mu_0$, then we denote $I(0, -\mu_0, \phi)$ as the downwards extraterrestrial radiation at the top of atmosphere(TOA), which can be expressed more rigorously as (Pelkowski 2007):

$$I(0, -\mu_0, \phi) = \frac{Q_0^\downarrow}{2} \delta(\mu + \mu_0) [1 - H(\mu)] \delta(\phi - \phi_0). \quad (2.8)$$

Q_0^\downarrow is the extraterrestrial downward irradiance, δ and H is the delta-function and the Heaviside step function respectively. Now, substituting $\tau_0 = 0$, $\mu = -\mu_0$ into Eq. (2.7) leads to:

$$I(\tau, \mu < 0, \phi) = I(0, -\mu_0, \phi)e^{\frac{\tau}{\mu}} - \frac{1}{\mu} \int_0^\tau S(\tau', \mu, \phi)e^{-\frac{\tau'-\tau}{\mu}} d\tau'. \quad (2.9)$$

The two terms on the right-hand side of Eq. (2.7) or (2.9) respectively represents the direct and the diffuse radiation in a medium, this separation of the radiation field could be expressed by:

$$I(\tau, \mu, \phi) = I^\odot(\tau, \mu, \phi) + I^*(\tau, \mu, \phi), \quad (2.10)$$

where I^\odot stands for the direct radiation, the radiation coming directly from the Sun's disk in the sky; and I^* stands for the diffuse radiation, the radiation field coming from any direction from the sky, after interaction with the medium. Boundary conditions at the TOA for I^\odot and I^* can be determined:

$$\begin{aligned} I^\odot(\tau = 0, \mu > 0, \phi) &= I^*(\tau = 0, \mu < 0, \phi) = 0, \\ I^\odot(\tau = 0, \mu < 0, \phi) &= I(0, -\mu_0, \phi). \end{aligned} \quad (2.11)$$

Comparing Eqs. (2.9) and (2.10), we might write the direct component as:

$$I^\odot(\tau, \mu < 0, \phi) = I(0, -\mu_0, \phi)e^{\tau/\mu}, \quad (2.12)$$

and the diffuse component as:

$$I^*(\tau, \mu < 0, \phi) = -\frac{1}{\mu} \int_0^\tau S(\tau', \mu, \phi)e^{-\frac{\tau'-\tau}{\mu}} d\tau'. \quad (2.13)$$

Notice that Eq. (2.12) is the solution of

$$\mu \frac{dI^\odot(\tau, \mu, \phi)}{d\tau} = I^\odot(\tau, \mu, \phi), \quad (2.14)$$

by applying the boundary condition at TOA. Eq. (2.14) is usually known as Beer-Lambert-Bouguer law. Replacing extraterrestrial radiation Eq. (2.8) into Eq. (2.12), we have the expression of direct radiation in a given optical depth τ :

$$I^\odot(\tau, \mu < 0, \phi) = Q_0^\downarrow \delta(\mu + \mu_0) \delta(\phi - \phi_0) e^{\frac{\tau}{\mu}}. \quad (2.15)$$

The diffuse component (Eq. (2.13)) that contains the source function S , to make physical sense, convergence is required:

$$\lim_{\tau \rightarrow \infty} S(\tau) e^{-\tau} \rightarrow 0. \quad (2.16)$$

S can be decomposed in the form:

$$S(\tau, \mu, \phi) = [1 - \tilde{\omega}(\tau)]B(\tau) + \frac{\tilde{\omega}(\tau)}{4\pi} \int_0^{2\pi} \int_{-1}^1 P(\tau, \mu, \phi, \mu', \phi') I(\tau, \mu', \phi') d\mu' d\phi'. \quad (2.17)$$

The first term on the right-hand side is the emission term, where $B(\tau)$ is Planck function, $\tilde{\omega} = 1 - \beta_a/\beta_e$ is called *single scattering albedo*, β_a is the absorption coefficient, $1 - \tilde{\omega}$ describes the absorption portion in an extinction event. If we do not care about longwave radiation on the basis of the fifth simplification, $B(\tau) \approx 0$ for shortwave range in our atmosphere, and then the emission term $[1 - \tilde{\omega}(\tau)]B(\tau)$ is neglected; the second term on the right-hand side is the scattering term, because of this term, we can see that the source function depends on I , which brings in a major difficulty to radiative transfer calculations. If we denote Θ as the scattering angle between incidence and observation directions, then,

$$\cos \Theta = \mathbf{\Omega} \cdot \mathbf{\Omega}' = \mu\mu' + (1 - \mu^2)^{1/2}(1 - \mu'^2)^{1/2} \cos(\theta - \theta'). \quad (2.18)$$

$P(\tau, \mu, \phi, \mu', \phi')$ is called the *scattering phase function*, describing the normalized angular energy distribution of a single scattering event without polarization. It can be expanded in Legendre polynomials by the addition theorem for spherical harmonics (Chandrasekhar 1960):

$$P(\mu, \theta, \mu', \theta') \approx \sum_{m=0}^N (2 - \delta_{0,m}) \left\{ \sum_{l=m}^N \varpi_l^m P_l^m(\mu) P_l^m(\mu') \right\} \cos m(\theta' - \theta), \quad (2.19)$$

where P_l^m is the associated Legendre polynomial, and

$$\varpi_l^m = \varpi_l \frac{(l-m)!}{(l+m)!} \quad (l = m, \dots, N, 0 \leq m \leq N), \quad \delta_{0,m} = \begin{cases} 1 & \text{if } m=0, \\ 0 & \text{otherwise.} \end{cases} \quad (2.20)$$

The zeroth moment of phase function, ϖ_0 , is equal to unity due to the normalization; the first moment is usually related to the *asymmetry factor* as $g = \varpi_1/3$, which describes to a great extent the symmetry of a scattering event.

Now, substituting Eqs. (2.8), (2.10) and (2.17) into Eq. (2.6), we get:

$$\begin{aligned} \mu \frac{dI^*(\tau, \mu, \phi)}{d\tau} &= I^*(\tau, \mu, \phi) - \frac{\tilde{\omega}(\tau)}{4\pi} Q_0^\downarrow P(\tau, \mu, \phi, -\mu_0, \phi_0) e^{-\frac{\tau}{\mu_0}} \\ &\quad - \frac{\tilde{\omega}(\tau)}{4\pi} \int_0^{2\pi} \int_{-1}^1 P(\tau, \mu, \phi, \mu', \phi') I^*(\tau, \mu', \phi') d\mu' d\phi', \end{aligned} \quad (2.21)$$

an integro-differential equation. On the right-hand side, the first term describes the attenuation by extinction processes, the second term is due to the primary scattering of the direct radiation, while the third term is associated with contributions of multiple scattering from the diffuse radiation. If then the sixth simplification is applied, Eq. (2.21) reduces to:

$$\mu \frac{dI^*(\tau, \mu)}{d\tau} = I^*(\tau, \mu) - \frac{\tilde{\omega}(\tau)}{4\pi} Q_0^\downarrow P(\tau, \mu, -\mu_0) e^{-\frac{\tau}{\mu_0}} - \frac{\tilde{\omega}(\tau)}{2} \int_{-1}^1 P(\tau, \mu, \mu') I^*(\tau, \mu') d\mu'. \quad (2.22)$$

The main task of the rest of this chapter is to tackle Eq. (2.22). It is customary to treat only the diffuse component in RTE, the direct component being estimated independently by Eq. (2.12) or (2.14). Instead of the requirement of data for τ , $\tilde{\omega}$ and P for solving Eq. (2.22), only τ is needed for calculation of the direct radiation.

2.2. An overview of the main approaches for solving the RTE

2.2.1. Discrete ordinates

The discrete ordinates approach, introduced by Chandrasekhar (1950), faces directly the RTE. Replacing the integral over μ' by a Gaussian quadrature formula, Eq. (2.22) can be dealt with numerically:

$$\begin{aligned} \mu_i \frac{dI^*(\tau, \mu_i)}{d\tau} = & I^*(\tau, \mu_i) - \frac{\tilde{\omega}(\tau)}{4\pi} Q_0^\downarrow P(\tau, \mu_i, -\mu_0) e^{-\frac{\tau}{\mu_0}} \\ & - \frac{\tilde{\omega}(\tau)}{2} \sum_{j=-n}^n a_j P(\tau, \mu_i, \mu_j) I^*(\tau, \mu_j), \quad (i = -n, \dots, n) \end{aligned} \quad (2.23)$$

I^* is then discretized to $2n$ “streams”, with μ_i chosen to be the zeros of the even-order Legendre polynomial $P_{2n}(\mu)$, whilst a_j ($j = -n, \dots, -1, 1, \dots, n$) are known as the Gaussian quadrature weights, which are given by:

$$a_j = \frac{1}{P'_{2n}(\mu_j)} \int_{-1}^1 \frac{P_{2n}(\mu)}{\mu - \mu_j} d\mu. \quad (2.24)$$

The zeros and weights satisfy $\mu_{-j} = -\mu_j$, and $a_{-j} = a_j$. Now define:

$$\begin{aligned} \alpha_{ij}(\tau) &= \frac{1}{\mu_i} \left[\delta_{ij} - \frac{\tilde{\omega}(\tau)}{2} a_j P(\tau, \mu_i, \mu_j) \right], \\ \beta_{ij}(\tau) &= -\frac{1}{\mu_i} \cdot \frac{\tilde{\omega}(\tau)}{2} a_j P(\tau, \mu_i, \mu_{-j}). \end{aligned} \quad (2.25)$$

Where δ_{ij} is the kronecker delta, from Eq. (2.18), we learn that the phase function respects Helmholtz’s law of reciprocity, namely,

$$P(\mu, -\mu') = P(-\mu, \mu'), \quad P(-\mu, -\mu') = P(\mu, \mu'). \quad (2.26)$$

Therefore, $\alpha_{-ij} = -\alpha_{i-j}$, $\alpha_{-i-j} = -\alpha_{ij}$, as well as $\beta_{-ij} = -\beta_{i-j}$, $\beta_{-i-j} = -\beta_{ij}$. If we assume the atmosphere to be homogeneous, i.e., $\tilde{\omega}$, P , α_{ij} and β_{ij} are independent of τ , and separate the upward and downward radiations, the homogeneous part of Eq. (2.23) becomes:

$$\begin{aligned}\frac{dI^{*\uparrow}(\tau, \mu_i)}{d\tau} &= \sum_{j=1}^n \alpha_{ij} I^{*\uparrow}(\tau, \mu_j) + \sum_{j=1}^n \beta_{ij} I^{*\downarrow}(\tau, \mu_{-j}), \\ \frac{dI^{*\downarrow}(\tau, \mu_{-i})}{d\tau} &= \sum_{j=1}^n (-\beta_{ij}) I^{*\uparrow}(\tau, \mu_j) + \sum_{j=1}^n (-\alpha_{ij}) I^{*\downarrow}(\tau, \mu_{-j}),\end{aligned}\tag{2.27}$$

and in compact matrix form:

$$\frac{d}{d\tau} \begin{bmatrix} \mathbf{I}^{*\uparrow}(\tau) \\ \mathbf{I}^{*\downarrow}(\tau) \end{bmatrix} = \begin{bmatrix} \boldsymbol{\alpha} & \boldsymbol{\beta} \\ -\boldsymbol{\beta} & -\boldsymbol{\alpha} \end{bmatrix} \begin{bmatrix} \mathbf{I}^{*\uparrow}(\tau) \\ \mathbf{I}^{*\downarrow}(\tau) \end{bmatrix},\tag{2.28}$$

where,

$$\begin{aligned}\mathbf{I}^{*\uparrow}(\tau) &= [I^*(\tau, \mu_1), I^*(\tau, \mu_2), \dots, I^*(\tau, \mu_n)], \\ \mathbf{I}^{*\downarrow}(\tau) &= [I^*(\tau, \mu_{-1}), I^*(\tau, \mu_{-2}), \dots, I^*(\tau, \mu_{-n})].\end{aligned}\tag{2.29}$$

By assuming solutions of the form $\mathbf{I}^{*\uparrow\downarrow} = \mathbf{g}^{\uparrow\downarrow} e^{-k\tau}$ for Eq. (2.28), we arrive at an eigenvalue problem:

$$\begin{bmatrix} \boldsymbol{\alpha} & \boldsymbol{\beta} \\ -\boldsymbol{\beta} & -\boldsymbol{\alpha} \end{bmatrix} \begin{bmatrix} \mathbf{g}^{\uparrow} \\ \mathbf{g}^{\downarrow} \end{bmatrix} = -k \begin{bmatrix} \mathbf{g}^{\uparrow} \\ \mathbf{g}^{\downarrow} \end{bmatrix}.\tag{2.30}$$

Next, as solutions of vectors $\mathbf{g}^{\uparrow} + \mathbf{g}^{\downarrow}$ and $\mathbf{g}^{\uparrow} - \mathbf{g}^{\downarrow}$ can be found by adding and subtracting two equations in Eq. (2.30), we can then obtain the eigenvectors $[\mathbf{g}^{\uparrow} \ \mathbf{g}^{\downarrow}]$. By Eq. (2.23), particular solution can be obtained of the form $I_p^*(\tau, \mu_j) = M_i e^{-\tau/\mu_0}$. The general solution can then be written as (Liou 1973):

$$I^*(\tau, \mu_i) = \sum_{j=-n}^n L_j g_j(\mu_i) e^{-k_j \tau} + M_i e^{-\frac{\tau}{\mu_0}},\tag{2.31}$$

where the constants L_j and M_i are to be determined from the boundary conditions.

2.2.2. Successive orders of scattering

Successive orders of scattering (Van de Hulst 1948; Busbridge 1960) is one of several iteration methods that can be adopted to solve integro-differential equations. The idea is simple: if we can get rid of the multiple scattering term in Eq. (2.22) in each iterative step, then an integro-differential equation becomes a differential equation. Its physical sense is that, from the original source, we just trace every single scattering event in medium step by step, and then sum them up to get the combined contribution. For more details see Appendix A.1.

2.2.3. Invariant imbedding

This approach, though it does not deal directly with RTE, seeks solutions by rigorous physical reasoning. It was originally introduced by astrophysicist Ambartsumian (1942) for a semi-infinite plane-parallel atmosphere, as *principles of invariance* (Sobolev 1963), then it was developed by Chandrasekhar (1960) to be applied in finite atmospheres. *Invariant imbedding* was generalized and “mathematized” by Bellman and Kalaba (1961). For more details see Appendix A.2.

2.2.4. Adding and doubling

This is a method that divides a plane-parallel atmosphere into multiple thin layers, with their own properties and eventually adds them up. When thin layers possess distinct optical properties, the process is called *adding*, otherwise it is called to *doubling*. The doubling method originated with Stokes (1862), but it was not until a century later that it was introduced into atmospheric radiation by Van de Hulst (1963), Twomey *et al.* (1966), etc. For more details see Appendix A.3.

2.2.5. Integral equation

It was used by Chandrasekhar (1960) and described by authors like Cheyney III and Arking (1976). Instead of focusing on I , attention is centered on the source function S , for which a Fredholm integral equation of the second kind can be set up (Thomas and Stamnes 2002). For isotropic scattering, and denoting S^* as source from the primary scattering, the source function is solution to a linear integral equation in one variable:

$$S(\tau) = S^*(\tau) + \frac{\tilde{\omega}(\tau)}{2} \int_0^{\tau_b} E_1(|\tau - \tau'|) S(\tau') d\tau', \quad (2.32)$$

which is called the *Schwarzschild-Milne* equation, whose kernel E_1 is the *exponential integral* of order 1. Various methods like Neumann series expansion can then be applied to find $S(\tau)$.

2.2.6. Feautrier method

By calculating from a density-like variable $u = 1/2(I^\uparrow + I^\downarrow)$, and a flux-like variable $v = 1/2(I^\uparrow - I^\downarrow)$ (cf. Eq. (2.27)), the RTE can be transformed into a second-order differential transport equation of $u(\tau)$:

$$\mu^2 \frac{d^2 u(\tau, \mu)}{d\tau^2} = u(\tau, \mu) - S(\tau). \quad (2.33)$$

This method was generalized by Feautrier (1964), more details can be found in the astrophysical monograph by Mihalas (1978).

2.2.7. Spherical harmonics

This idea, developed by Eddington (1926), is somewhat similar to *discrete ordinates*. It expands $I(\tau, \mu)$ in RTE in a series of Legendre polynomials $P_j(\mu)$:

$$I(\tau, \mu) = \sum_{j=0}^{\infty} P_j(\mu) I_j(\tau), \quad (2.34)$$

which forms a complete set of orthogonal functions in the interval $(-1, 1)$. The recurrence relation of Legendre polynomial can be used to obtain a system of linear differential equations (Kourganoff 1952). The simplest two-term expansion $I(\tau, \mu) = I_0(\tau) + \mu I_1(\tau)$ leads to one of so-called Eddington's approximations.

2.2.8. Monte Carlo

Monte Carlo for radiative transfer is a probabilistic method that simulates the stochastic processes of photons in a medium. Starting from an original source, all subsequent events of each photon depend on probability distribution functions (PDFs) at given positions, where the optical properties are predefined. Computation simulates a large amount of photons, the collective effect of the “random walk” of each photon approaching gradually “reality”. Finally, the emerging photons from an interested position can be counted. Algorithms and applications of the Monte Carlo method have been developed and used by Danielson *et al.* (1969); Plass and Kattawar (1971); Kattawar *et al.* (1973); Marchuk *et al.* (1980), etc.

2.2.9. Comparison among approaches

The approaches outlined above show a variety of radiative calculation methods, some of which share similarities, such as the connection between doubling and discrete ordinates (Stamnes 1986), the equivalence of the adding method and the principles of invariance (Liou 2002). Nonetheless, all these methods and many more have their advantages and drawbacks, and therefore their own applications.

Successive orders of scattering has a physically intuitive interpretation. However, in a thick ($\tau > 5$) and nearly conservative ($\tilde{\omega} \approx 1$) medium, it converges slowly (Van de Hulst 1980).

Invariant imbedding can be analytically reduced to simple form under isotropic conditions or even for Rayleigh scattering conditions, but when the phase function requires more than a few Legendre polynomials, the analytic characteristic functions $\Psi(\mu')$ (in Eqs. (A.14) and (A.15)) are less easy to calculate (Liou 2002).

Discrete ordinates solves the RTE directly in explicit form, unlike many iterative methods, and its procedures do not depend upon the optical thickness. The accuracy and capability

has been demonstrated by Liou (1973), but for a thick atmosphere huge and tiny matrix elements appear, leading to what is called *ill-conditioning* by Thomas and Stamnes (2002).

Adding and doubling is easily implemented for a medium of arbitrary optical depth, it has been successfully put to practical use by Van de Hulst (1980). Both *discrete ordinates* and *adding and doubling* are widely used to compute benchmark results with high accuracy (Zdunkowski *et al.* 2007).

Other methods like those for solving an *integral equation* or *Feautrier method* are more applicable to isotropic conditions and therefore are applied more frequently in astrophysics. *Monte Carlo* can be used to solve problems not restricted to plane-parallel medium, but is very demanding as to calculation time and not easy to model.

For our purposes, estimating irradiance relating to our results with atmospheric characteristics, a more flexible and faster computing approach is to be preferred. Since the “*ill-conditioning*” problem can be solved by the removal of positive exponentials through a scaling transformation (Stamnes and Conklin 1984), a full-fledged computer code DISORT using discrete ordinates has been developed successfully by Stamnes *et al.* (1988), and so discrete ordinates is chosen for our work. In the following section, we therefore need to look more deeply into this approach.

2.3. A deeper look into discrete ordinates

We take a closer look at Eq. (2.23), which basically builds a set of linear differential equations for $I^*(\tau, \mu_i)$ from the original RTE (2.22). Note that normally we deal only with diffuse radiation in RTE, so without fear of ambiguity superscript * may be dropped hereafter, for simplicity. Gaussian quadrature is commonly chosen for numerical integration, although Kourganoff (1952) argued that a Newton-Cotes type of formula provides more rapid convergence in lower orders of approximation. However, the *double-Gauss* method can avoid this problem (Stamnes *et al.* 1988), so we stick with Gaussian quadrature, as essentially there is no theoretical difference between quadrature of Gauss and double-Gauss.

In this section, we examine more of the details of two simpler but representative cases: isotropic scattering and two-stream approximation, along with some manipulation techniques.

2.3.1. Isotropic scattering

In the isotropic-scattering case, and considering only a homogeneous atmospheric layer, Eq. (2.23) becomes:

$$\mu_i \frac{I(\tau, \mu_i)}{d\tau} = I(\tau, \mu_i) - \frac{\tilde{\omega}}{4\pi} Q_0^\dagger e^{-\frac{\tau}{\mu_0}} - \frac{\tilde{\omega}}{2} \sum_{j=-n}^n a_j I(\tau, \mu_j). \quad (2.35)$$

Substitution of $I(\tau, \mu_i) = g_i e^{-k\tau}$ into the homogeneous part of Eq. (2.35) yields:

$$(1 + \mu_i k) g_i = \frac{\tilde{\omega}}{2} \sum_{j=-n}^n a_j g_j. \quad (2.36)$$

Since g_i and k are constants, we get the characteristic equation for eigenvalue k (Chandrasekhar 1960):

$$1 = \frac{\tilde{\omega}}{2} \sum_{j=-n}^n \frac{a_j}{1 + \mu_j k} = \tilde{\omega} \sum_{j=1}^n \frac{a_j}{1 - \mu_j^2 k^2}. \quad (2.37)$$

If the layer is non-conservative ($\tilde{\omega} < 1$), we get $2n$ nonzero eigenvalues, so the homogeneous general solution can be written by $2n$ linearly independent solutions:

$$I(\tau, \mu_i) = \sum_{j=-n}^n \frac{L_j}{1 + \mu_i k_j} e^{-k_j \tau}. \quad (2.38)$$

According to the property of Gaussian weights

$$\sum_{i=-n}^n a_i = 2, \quad (2.39)$$

for the conservative case ($\tilde{\omega} = 1$), and Eq. (2.37) only produces $2n - 2$ nonzero roots, so two more independent solutions are required (for more details see Chandrasekhar 1960; Kourganoff 1952). These eigenvalues can be thought of as effective extinction coefficients such that every $k_j \tau$ represents an effective optical path for each stream (Goody and Yung 1995; Liou 2002). By introducing Chandrasekhar's H function, defined as

$$H(\mu) = \frac{1}{\mu_1 \dots \mu_n} \frac{\prod_{i=1}^n (\mu + \mu_i)}{\prod_{\alpha=1}^{n-1} (1 + k_\alpha \mu)}, \quad (2.40)$$

we may find a particular solution to to Eq. (2.35). The H function is actually the semi-infinite limit case of the X function (cf. Eq. (A.14)), such that:

$$\lim_{\tau_b \rightarrow \infty} X(\mu) = H(\mu) = 1 + \mu H(\mu) \int_0^1 \frac{\Psi(\mu')}{\mu + \mu'} H(\mu') d\mu'. \quad (2.41)$$

The complete general solution can be expressed as (Chandrasekhar 1960; Liou 2002):

$$I(\tau, \mu_i) = \sum_{j=-n}^n \frac{L_j}{1 + \mu_i k_j} e^{-k_j \tau} + \frac{\tilde{\omega} Q_0^\downarrow H(\mu_0) H(-\mu_0)}{4\pi(1 + \mu_i/\mu_0)} e^{-\frac{\tau}{\mu_0}}. \quad (2.42)$$

2.3.2. Two-stream approximation

When the first-order Gaussian quadrature is carried out in discrete ordinates, we have what is known as the two-stream approximation. The two-stream approximation has a longer history, the original version dating back to the work by Schuster (1905) and Schwarzschild (1906).

In a homogeneous atmosphere, we rewrite Eq. (2.22) by distinguishing diffuse radiation of upper and lower hemisphere:

$$\begin{aligned} \mu \frac{dI^\uparrow(\tau, \mu)}{d\tau} &= I^\uparrow(\tau, \mu) - \frac{\tilde{\omega}}{4\pi} Q_0^\downarrow P(\mu, -\mu_0) e^{-\frac{\tau}{\mu_0}} \\ &\quad - \frac{\tilde{\omega}}{2} \int_{-1}^0 P(\mu, \mu') I^\downarrow(\tau, \mu') d\mu' - \frac{\tilde{\omega}}{2} \int_0^1 P(\mu, \mu') I^\uparrow(\tau, \mu') d\mu', \end{aligned} \quad (2.43)$$

$$\begin{aligned} \mu \frac{dI^\downarrow(\tau, \mu)}{d\tau} &= I^\downarrow(\tau, \mu) - \frac{\tilde{\omega}}{4\pi} Q_0^\downarrow P(\mu, -\mu_0) e^{-\frac{\tau}{\mu_0}} \\ &\quad - \frac{\tilde{\omega}}{2} \int_{-1}^0 P(\mu, \mu') I^\downarrow(\tau, \mu') d\mu' - \frac{\tilde{\omega}}{2} \int_0^1 P(\mu, \mu') I^\uparrow(\tau, \mu') d\mu'. \end{aligned} \quad (2.44)$$

Upon approximating

$$I^\uparrow = I^\uparrow(\tau) \approx \int_0^1 I^\uparrow(\tau, \mu) d\mu, \quad I^\downarrow = I^\downarrow(\tau) \approx \int_{-1}^0 I^\downarrow(\tau, \mu) d\mu, \quad (2.45)$$

and defining a particular μ_1 ,

$$\mu_1 = \bar{\mu}^\uparrow = \frac{\int_0^1 I^\uparrow(\tau, \mu) \mu d\mu}{\int_0^1 I^\uparrow(\tau, \mu) d\mu} \approx \frac{F^\uparrow}{2\pi I^\uparrow}, \quad -\mu_1 = \bar{\mu}^\downarrow = \frac{\int_{-1}^0 I^\downarrow(\tau, \mu) \mu d\mu}{\int_{-1}^0 I^\downarrow(\tau, \mu) d\mu} \approx -\frac{F^\downarrow}{2\pi I^\downarrow}, \quad (2.46)$$

we apply integration $\int_0^1 d\mu$ on Eq. (2.43) and $\int_{-1}^0 d\mu$ on Eq. (2.44), to get:

$$\mu_1 \frac{dI^\uparrow}{d\tau} = I^\uparrow - \tilde{\omega} \bar{b} I^\downarrow - \tilde{\omega} (1 - \bar{b}) I^\uparrow - \frac{\tilde{\omega} b(-\mu_0)}{2\pi} Q_0^\downarrow e^{-\frac{\tau}{\mu_0}}, \quad (2.47)$$

$$-\mu_1 \frac{dI^\downarrow}{d\tau} = I^\downarrow - \tilde{\omega} (1 - \bar{b}) I^\downarrow - \tilde{\omega} \bar{b} I^\uparrow - \frac{\tilde{\omega} [1 - b(-\mu_0)]}{2\pi} Q_0^\downarrow e^{-\frac{\tau}{\mu_0}}, \quad (2.48)$$

where the backscattering coefficients $b(\mu')$ and \bar{b} are given by:

$$b(\mu') = \begin{cases} \frac{1}{2} \int_{-1}^0 P(\mu, \mu') d\mu & \mu' > 0 \\ \frac{1}{2} \int_0^1 P(\mu, \mu') d\mu & \mu' < 0 \end{cases} \quad 1 - b(\mu') = \begin{cases} \frac{1}{2} \int_0^1 P(\mu, \mu') d\mu & \mu' > 0 \\ \frac{1}{2} \int_{-1}^0 P(\mu, \mu') d\mu & \mu' < 0 \end{cases} \quad (2.49)$$

$$\bar{b} = \begin{cases} \frac{\int_{-1}^0 b(\mu') I^\downarrow(\tau, \mu') d\mu'}{\int_{-1}^0 I^\downarrow(\tau, \mu') d\mu'} & \mu' < 0 \\ \frac{\int_0^1 b(\mu') I^\uparrow(\tau, \mu') d\mu'}{\int_0^1 I^\uparrow(\tau, \mu') d\mu'} & \mu' > 0 \end{cases} \quad 1 - \bar{b} = \begin{cases} \frac{\int_{-1}^0 [1 - b(\mu')] I^\downarrow(\tau, \mu') d\mu'}{\int_{-1}^0 I^\downarrow(\tau, \mu') d\mu'} & \mu' < 0 \\ \frac{\int_0^1 [1 - b(\mu')] I^\uparrow(\tau, \mu') d\mu'}{\int_0^1 I^\uparrow(\tau, \mu') d\mu'} & \mu' > 0 \end{cases} \quad (2.50)$$

here the definition from Wiscombe and Grams (1976) is adopted, that $b(\mu')$ describes contribution from intensity of a given direction μ' to the opposite hemisphere, whilst many other authors, like Coakley Jr. and Chýlek (1975) and Thomas and Stamnes (2002), give a reverse description, defining $b(\mu)$ as contribution from intensity of backward hemisphere to a designated direction μ , which is not adopted by the present author in the context of two-stream approximation.

Now we look for consistency with discrete ordinates. In Eqs. (2.19) and (2.20), when $m = 0$ (azimuthal average or independence), truncating the expansion to $l \leq 1$ leads to:

$$P(\mu_1, \mu'_1) \approx 1 + \varpi_1 \mu_1 \mu'_1 = 1 + 3g\mu_1 \mu'_1, \quad (2.51)$$

According to the first-order Gaussian quadrature,

$$a_1 = a_{-1} = 1, \quad \mu_1 = \frac{1}{\sqrt{3}}, \quad \mu_{-1} = -\mu_1 = -\frac{1}{\sqrt{3}}. \quad (2.52)$$

Note that, the value $\mu_1 = 1/\sqrt{3}$, sometimes is referred to as the diffusivity factor, which agrees with discrete ordinates. However, it is not the only choice, many authors have their own tuning selections in different two-stream variants. More details, along with the range of choices for μ_1 , can be found in a discussion by Pelkowski (2007, 2009). Additionally, under the two-stream approximation, we might denote:

$$P(\mu_1, \mu') = \int_0^1 P(\mu, \mu') d\mu, \quad P(\mu_{-1}, \mu') = P(-\mu_1, \mu') = \int_{-1}^0 P(\mu, \mu') d\mu. \quad (2.53)$$

Then from Eqs. (2.49) to (2.53), we obtain:

$$\bar{b} = b \left(\pm \frac{1}{\sqrt{3}} \right) \approx \frac{1-g}{2}, \quad (2.54)$$

which is consistent with the assumption by Sagan and Pollack (1967). Now, by comparing with Eqs. (2.25) and (2.27), when $i = j = 1$, the equivalence between the earliest two-stream approximation and the Gaussian quadrature approach can be found (cf. Eqs. (2.52) to (2.54)):

$$\begin{aligned} \pm \alpha_{11} &= \pm \frac{1 - \tilde{\omega}(1 - \bar{b})}{\mu_1} = \pm \frac{1}{\mu_1} \left[1 - \frac{\tilde{\omega}(1+g)}{2} \right], \\ \pm \beta_{11} &= \mp \frac{\tilde{\omega}\bar{b}}{\mu_1} = \mp \frac{1}{\mu_1} \cdot \frac{\tilde{\omega}(1-g)}{2}. \end{aligned} \quad (2.55)$$

Based on the foregoing relationships, we rewrite Eqs. (2.47) and (2.48) as:

$$\mu_1 \frac{dI^\uparrow}{d\tau} = \left[1 - \frac{\tilde{\omega}(1+g)}{2} \right] I^\uparrow - \frac{\tilde{\omega}(1-g)}{2} I^\downarrow - \frac{\tilde{\omega}Q_0^\downarrow}{4\pi} (1 - 3g\mu_0\mu_1) e^{-\frac{\tau}{\mu_0}}, \quad (2.56)$$

$$-\mu_1 \frac{dI^\downarrow}{d\tau} = \left[1 - \frac{\tilde{\omega}(1+g)}{2} \right] I^\downarrow - \frac{\tilde{\omega}(1-g)}{2} I^\uparrow - \frac{\tilde{\omega}Q_0^\downarrow}{4\pi} (1 + 3g\mu_0\mu_1) e^{-\frac{\tau}{\mu_0}}. \quad (2.57)$$

By adding and subtracting Eqs. (2.56) and (2.57), we find the coupled equations of $I^\uparrow - I^\downarrow$ and $I^\uparrow + I^\downarrow$:

$$\frac{d^2(I^\uparrow - I^\downarrow)}{d\tau^2} = \Gamma^2(I^\uparrow - I^\downarrow) + M_1^* e^{-\frac{\tau}{\mu_0}}, \quad (2.58)$$

$$\frac{d^2(I^\uparrow + I^\downarrow)}{d\tau^2} = \Gamma^2(I^\uparrow + I^\downarrow) - M_2^* e^{-\frac{\tau}{\mu_0}}, \quad (2.59)$$

where

$$\Gamma^2 = \frac{(1 - \tilde{\omega})(1 - \tilde{\omega}g)}{\mu_1^2}, \quad (2.60)$$

and

$$\begin{aligned} M_1^* &= (1 - \tilde{\omega}) \frac{3g\mu_0\mu_1\tilde{\omega}Q_0^\downarrow}{2\pi\mu_1^2} + \frac{\tilde{\omega}Q_0^\downarrow}{2\pi\mu_0\mu_1}, \\ M_2^* &= (1 - \tilde{\omega}g) \frac{\tilde{\omega}Q_0^\downarrow}{2\pi\mu_1^2} + \frac{3g\tilde{\omega}Q_0^\downarrow}{2\pi}. \end{aligned} \quad (2.61)$$

Seeking general solutions to the homogeneous part in the form $I^{\uparrow\downarrow} = g^{\uparrow\downarrow} e^{-k\tau}$, as well the particular solutions in the form $I_p^{\uparrow\downarrow} = M^{\uparrow\downarrow} e^{-\frac{\tau}{\mu_0}}$, leads to the eigenvalues:

$$k_{\pm 1} = \pm \Gamma = \pm \frac{\sqrt{(1 - \tilde{\omega})(1 - \tilde{\omega}g)}}{\mu_1}, \quad (2.62)$$

and a relationship of the eigenvectors:

$$\frac{g_{-1}^{\downarrow}}{g_{-1}^{\uparrow}} = \frac{g_1^{\uparrow}}{g_1^{\downarrow}} = \gamma_{\infty} = \frac{\sqrt{1 - \tilde{\omega}g} - \sqrt{1 - \tilde{\omega}}}{\sqrt{1 - \tilde{\omega}g} + \sqrt{1 - \tilde{\omega}}}, \quad (2.63)$$

here γ_{∞} has its own physical meaning, which represents the albedo of a semi-infinite atmosphere (Petty 2006). The solutions are:

$$I^{\uparrow} = L_1 e^{\Gamma\tau} + \gamma_{\infty} L_2 e^{-\Gamma\tau} + M^{\uparrow} e^{-\frac{\tau}{\mu_0}}, \quad (2.64)$$

$$I^{\downarrow} = \gamma_{\infty} L_1 e^{\Gamma\tau} + L_2 e^{-\Gamma\tau} + M^{\downarrow} e^{-\frac{\tau}{\mu_0}}, \quad (2.65)$$

where

$$M^{\uparrow} = \frac{\mu_0^2}{2(1 - \mu_0^2 \Gamma^2)} (M_1^* + M_2^*), \quad M^{\downarrow} = \frac{\mu_0^2}{2(1 - \mu_0^2 \Gamma^2)} (M_1^* - M_2^*), \quad (2.66)$$

and L_1 and L_2 are two constants that depend on boundary conditions. For a black surface,

$$I^{\downarrow}(0) = 0, \quad I^{\uparrow}(\tau_b) = 0, \quad (2.67)$$

we can get:

$$L_1 = \frac{M^{\downarrow} \gamma_{\infty} e^{-\Gamma\tau_b} - M^{\uparrow} e^{-\frac{\tau_b}{\mu_0}}}{e^{\Gamma\tau_b} - \gamma_{\infty}^2 e^{-\Gamma\tau_b}}, \quad L_2 = \frac{M^{\uparrow} \gamma_{\infty} e^{-\frac{\tau_b}{\mu_0}} - M^{\downarrow} e^{\Gamma\tau_b}}{e^{\Gamma\tau_b} - \gamma_{\infty}^2 e^{-\Gamma\tau_b}}. \quad (2.68)$$

For a non-black surface, if we assume as an approximation Lambertian reflection, which means radiation is reflected irrespectively of direction, the boundary conditions are given by (Thomas and Stamnes 2002):

$$I^{\downarrow}(0) = 0, \quad I^{\uparrow}(\tau_b) = \rho_L \left[\mu_0 Q_0^{\downarrow} e^{-\frac{\tau_b}{\mu_0}} + 2\pi \mu_1 I^{\downarrow}(\tau_b) \right], \quad (2.69)$$

where ρ_L refers to the surface Lambertian reflectance, or can be thought of as the surface albedo, then:

$$L_1 = \frac{M^{\downarrow} C_3 e^{-\Gamma\tau_b} - C_4 e^{-\frac{\tau_b}{\mu_0}}}{C_1 e^{\Gamma\tau_b} + C_2 e^{-\Gamma\tau_b}}, \quad L_2 = \frac{-M^{\downarrow} C_1 e^{-\Gamma\tau_b} + \gamma_{\infty} C_4 e^{-\frac{\tau_b}{\mu_0}}}{C_1 e^{\Gamma\tau_b} + C_2 e^{-\Gamma\tau_b}}, \quad (2.70)$$

where

$$\begin{aligned} C_1 &= 2\pi \gamma_{\infty} \rho_L \mu_1 - 1, & C_2 &= \gamma_{\infty}^2 - 2\pi \gamma_{\infty} \rho_L \mu_1, \\ C_3 &= 2\pi \rho_L \mu_1 - \gamma_{\infty}, & C_4 &= 2\pi M^{\downarrow} \rho_L \mu_1 - M^{\uparrow} + Q_0^{\downarrow} \rho_L \mu_0. \end{aligned} \quad (2.71)$$

Note that in the two-stream approximation, by utilizing $F^{\uparrow\downarrow} = 2\pi\mu_1 I^{\uparrow\downarrow}$ in Eq. (2.46), irradiance can later readily be obtained.

For higher order of discrete ordinates, or, more streams (2^n , $n > 1$), I^\uparrow and I^\downarrow in Eq. (2.45) will be replaced by vectors in Eq. (2.29), and matrix manipulation is needed (Stamnes and Conklin 1984; Nakajima and Tanaka 1986), although analytic solutions for four-stream ($n = 2$) can be derived in closed forms (Liou 1974).

2.3.3. Inhomogeneous atmosphere

The discussions above are for a homogeneous layer. For realistic applications, inhomogeneity should be considered. A similar strategy could be taken up as the *adding method* (see Section 2.2.4 and Appendix A.3) to deal with the inhomogeneity, by regarding the atmosphere as a stack of several homogeneous layers, each layer being characterized by its own thickness, single scattering albedo and phase function. Then solutions in the form of Eq. (2.31) can be concatenated, with the constants determined by boundary conditions (Liou 1975). We identify variables of each layer by superscript l , where $l = 1, 2, \dots, L$, and $\tau^l = \tau_{l+1} - \tau_l$, at the bottom of the atmosphere $\tau_b = \tau_L$.

First we rewrite Eq. (2.69) in an n -stream case:

$$I^1(0) = 0, \quad I^L(\tau_L, \mu_i) = \rho_L \left[\mu_0 Q_0^\downarrow e^{-\frac{\tau_L}{\mu_0}} + 2\pi \sum_{j=1}^n a_j I^L(\tau_L, \mu_{-j}) \mu_j \right], \quad (2.72)$$

The rest of conditions are determined by the continuity at interfaces between layers:

$$I^l(\tau_l, \mu_i) = I^{l+1}(\tau_l, \mu_i), \quad (l = 1, 2, \dots, L - 1) \quad (2.73)$$

Substituting Eq. (2.31) into Eqs. (2.72) and (2.73) leads to:

$$\begin{aligned} \sum_{j=-n}^n L_j^1 g_j^1(\mu_{-j}) &= -M_j^1, \\ \sum_{j=-n}^n \left[L_j^l g_j^l(\mu_j) e^{-k_j^l \tau^l} - L_j^{l+1} g_j^{l+1}(\mu_i) \right] &= -(M_i^l - M_i^{l+1}) e^{-\frac{\tau^l}{\mu_0}}, \\ \sum_{j=-n}^n L_j^L \left[g_j^L(\mu_{+i}) - 2\pi \rho_L \sum_{p=1}^n g_j^L(\mu_{-p}) a_p \mu_p \right] e^{-k_j^L \tau^L} & \\ &= \left(\rho_L \mu_0 Q_0^\downarrow e^{-\frac{\tau^L}{\mu_0}} + 2\pi \rho_L \sum_{j=1}^n M_{-j}^L a_j \mu_j - M_{+i}^L \right) e^{-\frac{\tau^L}{\mu_0}}. \end{aligned} \quad (2.74)$$

The remaining task is to determine $2n \times L$ coefficients L_j^l by the linear equation system, Eq. (2.74).

2.3.4. Scaling of phase function

In the application of discrete ordinates, the phase function is usually expressed as a Legendre expansion:

$$P(\cos \Theta) \approx \sum_{n=0}^N (2n+1) \chi_n P_n(\cos \Theta), \quad (2.75)$$

or in an azimuthal average, from Eqs. (2.18) to (2.20), in the form:

$$P(\mu, \mu') \approx \sum_{n=0}^N (2n+1) \chi_n P_n(\mu) P_n(\mu'). \quad (2.76)$$

Scattering by an aerosol, composed of larger particles compared to the wavelength of interacting light, has a strong forward peak, requiring at least hundreds of terms in Eq. (2.76) to represent a relatively accurate phase function. According to Thomas and Stamnes (2002), a similar number of streams in discrete ordinates is advised, which makes the computation even more unwieldy.

A popular group of treatments can be reduced to a truncation method called δ - M of Wiscombe (1977), whose expression (defining f as the truncation factor) is given by:

$$P'(\mu, \mu') = 2f\delta(\mu - \mu') + (1-f) \sum_{n=0}^{2M-1} (2n+1) \chi'_n P_n(\mu) P_n(\mu'). \quad (2.77)$$

This transformation is equivalent to “truncating” the forward-peak portion of the phase function to approximate by a delta-function, and this portion is treated as unscattered. χ'_n and f are chosen as:

$$\chi'_n = \frac{\chi_n - f}{1-f}, \quad (n = 0, \dots, 2M-1) \quad f = \chi_{2M}, \quad (n \geq 2M) \quad (2.78)$$

By a property of the delta-function (Morse and Feshbach 1953)

$$\delta(\mu - \mu') = \frac{1}{2} \sum_{n=0}^{\infty} (2n+1) P_n(\mu) P_n(\mu'), \quad (2.79)$$

the error incurred by the δ - M transformation can be obtained:

$$\varepsilon = P(\mu, \mu') - P'(\mu, \mu') = \sum_{n=2M}^{\infty} (\chi_n - f)(2n+1) P_n(\mu) P_n(\mu'), \quad (2.80)$$

so it reduces the error from the approximation of the ordinary phase function expansion by a portion of f . Instead of $\chi_n = 0$ for $n > 2M$, now $\chi_n = f = \chi_{2M}$ for $n > 2M$. After the transformation, we have,

$$d\tau' = (1 - \tilde{\omega}f)d\tau, \quad \tilde{\omega}' = \frac{1 - f}{1 - \tilde{\omega}f}\tilde{\omega}. \quad (2.81)$$

The reduction of optical depth is understandable because the forward-peak is regarded as not being scattered. Seeking effective optical depth and single scattering albedo like in Eq. (2.81) is generalized to similarity relations by Van de Hulst (1980). McKellar and Box (1981) also proved that δ - M as well as other transformations like δ -*Eddington* (Joseph *et al.* 1976), can be classified into a scaling group, where

$$\tau = \beta\tau'. \quad (2.82)$$

To maintain invariance in transformation, the new single scattering albedo and Legendre polynomial weights entail the following relationship with the original ones:

$$1 - \tilde{\omega}' = \beta(1 - \tilde{\omega}), \quad 1 - \tilde{\omega}'\chi'_n = \beta(1 - \tilde{\omega}\chi_n). \quad (2.83)$$

In the case of δ - M ,

$$\beta = (1 - \tilde{\omega}f)^{-1}. \quad (2.84)$$

Lin *et al.* (2018) introduced an improved δ - M + method, replacing the rather coarse treatment of setting $\chi_n = \chi_{2M}$ for all $n > 2M$ by modifying the expansion weights of delta-function with a factor of a Gaussian distribution, gaining much better results. δ - M + has been implemented into the latest version of the DISORT code.

2.4. Application and minimal layering of atmosphere

To put all this into practice, there is still more work to do. For our objective—the downward flux at the surface, the strategy is to design a model as economical as possible, using as few parameters as possible. The reason is very simple: information available is scanty.

As mentioned in Section 2.1, we simplify the radiative interaction as a grey process, that is, in each homogeneous layer, only *one* value of single scattering albedo, optical depth, or phase function needs to be assigned. Furthermore, the complicated Mie-scattering phase function can be replaced by the widely used Henyey-Greenstein phase function P_{HG} (Henyey and Greenstein 1941), by choosing the Legendre expansion weights $\chi_n = g^n$ in Eq. (2.75), and so a simple analytic form can be found:

$$P_{HG}(\cos \Theta) = \sum_{n=0}^{\infty} (2n + 1)g^n P_n(\cos \Theta) = \frac{1 - g^2}{(1 + g^2 - 2g \cos \Theta)^{3/2}}. \quad (2.85)$$

In the Henyey-Greenstein phase function, only the first moment or asymmetry factor g of the phase function appears. Although this is an approximate treatment, the multiple scattering

process and the integral calculation for obtaining irradiance will smooth out the results. By the way, the same guiding principle as with the grey simplification, the purpose here is not to discover and employ precise parameters, which are beyond our reach, but to keep only the essential physics, by choosing reasonable parameters in our pragmatic scheme. One scattering parameter is enough for grey simplification. The parameters in each layer to be specified are $\tilde{\omega}$, τ and g .

The next question is how to subdivide our atmosphere into certain number of homogeneous layers. Theoretically, our inhomogeneous atmosphere should be divided into an infinite number of layers, but here we have to find a feasible scheme. Pelkowski (2007, 2009) designed a tri-layered atmosphere, which divides the atmosphere into three layers: 1) an upper layer: the cloud-free atmosphere above the tropopause (or more generally above any significant cloud formation, since sometimes severe cumulonimbus' anvil can overshoot into the stratosphere); 2) a middle layer: the free troposphere, or the thermodynamically active layer, where the clouds form; 3) a lower layer: the boundary layer below the cloud base.

Let us examine these three layers one by one.

The upper layer has lower air density and is almost free of aerosols, except for dramatic events like volcanic eruptions, so optical variables are relatively stable, fluctuations do not affect daily estimations. Scattering in this layer will be treated as of Rayleigh type, such that $g = 0$. Ozone content needs to be considered when accounting for absorption of solar radiation.

The middle layer is most problematic, where capricious clouds form, with their irregular and discontinuous distribution, which is neither vertically nor horizontally homogeneous. Inside and outside clouds, there are utterly distinct optical properties: within the cloud, absorption of visible light is weak and the scattering of cloud droplets is strongly asymmetric; if the optical depth of a cloud is large, a photon might experience a great number of scattering events before it emerges from it; whilst outside the cloud, or in the interstices, the properties fall in somewhere between the upper layer and lower layer. The effective optical depth of this layer should be overall the largest of the three layers.

The lower layer is optically less dynamic than the middle layer, but compared with the upper layer and interstices of the middle layer, it has higher air density, contains normally more water vapor and aerosols. The amounts of water vapor and aerosols could be due to small or large scale weather system and local anthropogenic activity, hence vary discernibly during the day.

This reasonable layering scheme will be adopted, since more layers, say, even just 4, will *not* improve any performance of estimation owing to the lack of information; but layers less than 3 is far too simple to sufficiently render the realistic complexity of the radiative contribution. In any case, the main difficulty arises when all these variables have to be defined, especially

the estimation of optical depths of the middle and lower layers. The practical choices and relative discussions of $\tilde{\omega}$, τ and g in the tri-layered model will be left to Chapter 5, when numerical experiments are carried out.



Figure 2-1.: Early morning air pollution trapped in boundary layer (the lower layer) by inversion. (Photographed by the author in Bogotá, September 1st at 06:49 am, 2017.)

3. Statistics-driven approaches: empirical and neural network

3.1. Why do we need them?

The complexity of radiative calculations arises from our very atmosphere. Macroscopically, even if our atmosphere were well stratified, it is still a ceaselessly moving fluid, giving rise to a constantly changing structure, which complicates the vertical distribution. Particle density and composition at a certain altitude directly modify the behavior of electromagnetic waves passing through it. On the other side, microscopically, different particles affect electromagnetic waves of different frequencies, and molecular properties in absorption bands and scattering properties determine a phase function and extinction coefficient.

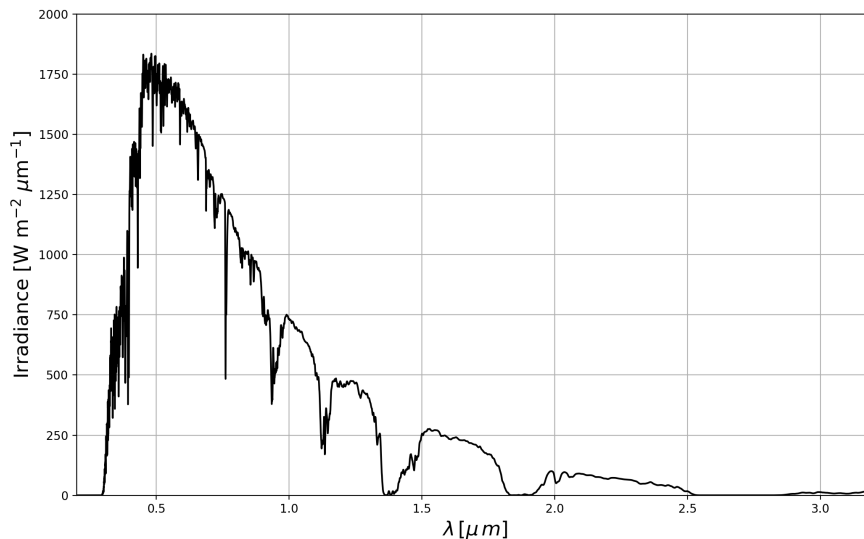


Figure 3-1.: Spectral distribution of surface irradiance by direct solar rays of zero zenith angle for a classic tropical atmosphere. (Generated by LOWTRAN 7, the elevation is set to 2600 meters above the sea level, approximately the altitude of Bogotá.)

As a whole, there are numerous factors that should be taken into account. Apart from the field of remote sensing or other particular purposes where line-by-line integration is employed,

it is too cumbersome to collect all the information for surface global irradiance. Fig. 3-1 shows the complexity of direct spectral irradiance for tropical atmosphere, not considering diffuse irradiance in cloudless or clouded condition. Even if a large number of simplifications have been imposed in the previous chapter, there is still room for practical approaches. In this chapter, empirical regression approaches and artificial intelligence techniques will be discussed.

3.2. Empirical approaches

It is not easy to categorize the countless empirical models. Authors like Bakirci (2009) distinguish models on the basis of mathematical form, other authors like Besharat *et al.* (2013) divide them by parameters which the model makes use of. In this section, we believe that the long-established Ångström–Prescott model and its varieties are worth discussing separately, with models that use cloudiness sharing a similar form, so we classify them together with Ångström–Prescott-type models; there are many other models which rely on variables other than sunshine duration or cloudiness, and we review them afterwards; then, a group of models which focuses on direct irradiance estimation will be discussed, too.

3.2.1. Ångström–Prescott-type models

First of all, we define a variable H ,

$$H(\Delta t, \Delta\mu) = \int_{\Delta t} \int_{\Delta\mu} Q_{\nu} d\nu dt, \quad (3.1)$$

with the unit $[J \cdot m^{-2} \cdot \Delta\mu^{-1} \cdot \Delta t^{-1}]$ standing for energy per unit square of area, received in a spectral range and a time range. Practically, the spectral range $\Delta\mu$ is usually set to be the effective range of irradiance detector deployed, and Δt to be a day. Unless otherwise stated, hereafter we will regard H as daily global solar irradiance, or *daily irradiance* without writing Δt and $\Delta\mu$.

Ångström (1924) suggested the linear relationship between daily irradiance and sunshine duration (see also the earlier attempt by Kimball (1919)). The modification later by himself (Ångström 1956) provided a general form:

$$\frac{H_g^{\downarrow}}{H_c^{\downarrow}} = \alpha + (1 - \alpha)\sigma, \quad (3.2)$$

where σ refers to the relative sunshine duration, whose value varies from $\sigma = 0$ for a fully overcast day, to $\sigma = 1$ for a entirely clear day, H_g^{\downarrow} represents the predicted daily irradiance on the ground, H_c^{\downarrow} represents the daily irradiance under a clear sky condition at the same location and the same time range. In such condition, $H_g^{\downarrow} = H_c^{\downarrow}$ complying with Eq. (3.2). On the other side, Ångström suggested $\alpha = 0.25$, which implies that for a wholly overcast day,

H_g^\downarrow would take on one quarter of the value of H_c^\downarrow . Nevertheless, definition of H_c^\downarrow brings in vagueness to a certain extent, a review by Martínez-Lozano *et al.* (1984) listed four possible interpretations. To avoid the problem of interpretation, Prescott (1940) instead used a more stable parameter—daily extraterrestrial downward irradiance H_0^\downarrow (cf. the definition of Q_0^\downarrow in Section 2.1) to replace it, proposing an equation in the form:

$$k = \frac{H_g^\downarrow}{H_0^\downarrow} = a + b\sigma, \quad (3.3)$$

where $a = 0.25$, $b = 0.54$ on his data analysis, k is the daily *clearness index*, or transparency. By this modification, $H_g^\downarrow = 0.79H_0^\downarrow$ for a perfectly sunny day, and $H_g^\downarrow = 0.25H_0^\downarrow$ for a wholly overcast day. Eq. (3.3) is the most basic form of Ångström–Prescott equation, it links the sunshine duration and the clearness index by a linear relationship. Because of the simplicity—only σ is required a lot of efforts based on this equation have been made in quest of best results.

One could easily get lost in the ocean of varieties of Ångström–Prescott-type models that have been published, hundreds of trimmed forms or modifications have been summarised by Martínez-Lozano *et al.* (1984); Bakirci (2009); Besharat *et al.* (2013); Despotovic *et al.* (2015) etc., ranging from linear, quadratic and cubic equations, to those mingled with trigonometric functions which relate to solar declination (see Section 4.1) or latitude. Nonetheless, all these models share a common feature that they all use sunshine duration. Yet, in our opinion, another group of models using cloudiness degree η —the average fractional total cloud amount recorded subjectively—should be counted as Ångström–Prescott type as well. Since these two variables, though one is time-based and the other is space-based, could conceivably hold a close relationship, which has been studied by a number of authors: some accept the approximation of a linear relationship like $\eta = 1 - \sigma$ (Kondratyev 1969; Brutsaert 1982), or do so with an expedient definition of cloudiness (Hoyt 1977); others dabble in special analyses trying to discover relatively sophisticated empirical relationships (Biga and Rosa 1980; Harrison and Coombes 1986; Bădescu 1990, 1991).

In some advanced versions, a and b themselves are set to be functions of day of the year, latitude, elevation, solar altitude, temperature, precipitation, or even σ as well (Glover and McCulloch 1958; Driedger and AJ 1970; Neuwirth 1980; Sfeir 1981; Frère 1975; Rietveld 1978; McEntee 1980; Gariepy 1980; Gopinathan 1988). However, these models could also be viewed as belonging to the group that we are going to talk about next.

3.2.2. Models involving other meteorological variables

Although sunshine duration and cloudiness are the variables that are most directly related to surface global irradiance, these data or observations are not available everywhere, at least not as common as such variables like temperature or humidity, or some other crucial

meteorological variables. Hargreaves and Samani (1982) came up with the idea of using the difference value between daily maximum and minimum temperature to guess the clearness index:

$$k = a(T_{max} - T_{min})^{0.5}. \quad (3.4)$$

This approach later was adopted and developed by many authors like Bristow and Campbell (1984), Allen (1997), Hunt *et al.* (1998), Meza and Varas (2000), Annandale *et al.* (2002), Mahmood and Hubbard (2002), Chen *et al.* (2004), among others. Beyond the Ångström–Prescott-type models, the temperature-dependent regression models have become most widely used.

Other authors argued that surface global irradiance should also be related to variables as relative humidity, precipitation, pressure, or water vapor content (Swartman and Ogunlade 1967; Lewis 1983; Ododo *et al.* 1995; Thornton and Running 1999; Maghrabi 2009).

3.2.3. Direct irradiance models

Even if most of the models take the typical H_0^\downarrow as in Eq. (3.3), H_c^\downarrow (in Eq. (3.2)) still appears in some models (e.g., Toğrul *et al.* 2000, and Bakirci 2008), thus the estimation for H_c^\downarrow itself becomes meaningful. Besides, the direct irradiance itself is essential for some application like concentrated solar power systems (Gueymard 2003a).

Leckner (1978) propounded a formula that reads:

$$H_\nu^\downarrow = H_{0\nu}^\downarrow \mathcal{T}_{r\nu} \mathcal{T}_{o\nu} \mathcal{T}_{g\nu} \mathcal{T}_{w\nu} \mathcal{T}_{a\nu}. \quad (3.5)$$

This equation describes how extraterrestrial irradiance abates when it passes through the atmosphere, or more specifically, how the direct part of irradiance is affected by five major constituents in the air (cf. Fig. 3-1). Notice the subscript ν in the equation, which means the calculation is to be done for each spectral interval, \mathcal{T}_ν indicates the spectral transmissivity, and subscript r , o , g , w and a correspondingly denotes Rayleigh particles, ozone, mixed gases, water vapor and aerosols. Later, Bird and Riordan (1986) developed a version based on Eq. (3.5). Nonetheless, more commonly used are broadband models, which do not distinguish the transmissivities of each constituents by frequency. Most of the broadband models share forms akin to Eq. (3.5), the modifications being largely made about the specialization of “mixed gases” as empirical equations for estimation of each transmissivity. Extensive work of review and performance comparison has been published by Gueymard (1993, 2003a,b).

3.3. Artificial intelligence technique

As a relatively new technique, artificial neural network, an artificial intelligence technique, may provide an alternative approach to estimate insolation. The nomenclature of neural network was inspired by neurobiological mechanisms of the brain. In contrast to traditional methods, the relationship between inputs and outputs is not pre-determined, but is the target itself; instead of calculating outputs from inputs and their relationship, the machine “learns” the relationship from samples of input and output variables, though this relationship, if any, will be enciphered in a batch of less meaningful numbers. The basic structure of an artificial neural network, consists of an input layer, an output layer, and single or multiple hidden layer/layers in between. Each layer is made of neurons, every one of which is associated with an output number, called *activation*. In a *feed-forward neural network*, each neuron has connection to all neurons in the adjacent layers, all connections having *weights*, the collection of which in a network represents the relationship between inputs and outputs that the network learns through training. The activation of a neuron is achieved by applying an *activation function* to the sum of its received signals, which are the results of the dot product of all the previous layer’s activations (if the previous layer is the input layer, then activations are equal to inputs), and weights of the corresponding connections to this neuron. The learning process is normally first to search for the error contributions of all weights by *back-propagation*, short for “backward propagation of errors”, which starts from the output errors, calculating backwards layer by layer; then doing *gradient descent*, which updates weights based on their error contributions, towards lower output errors.

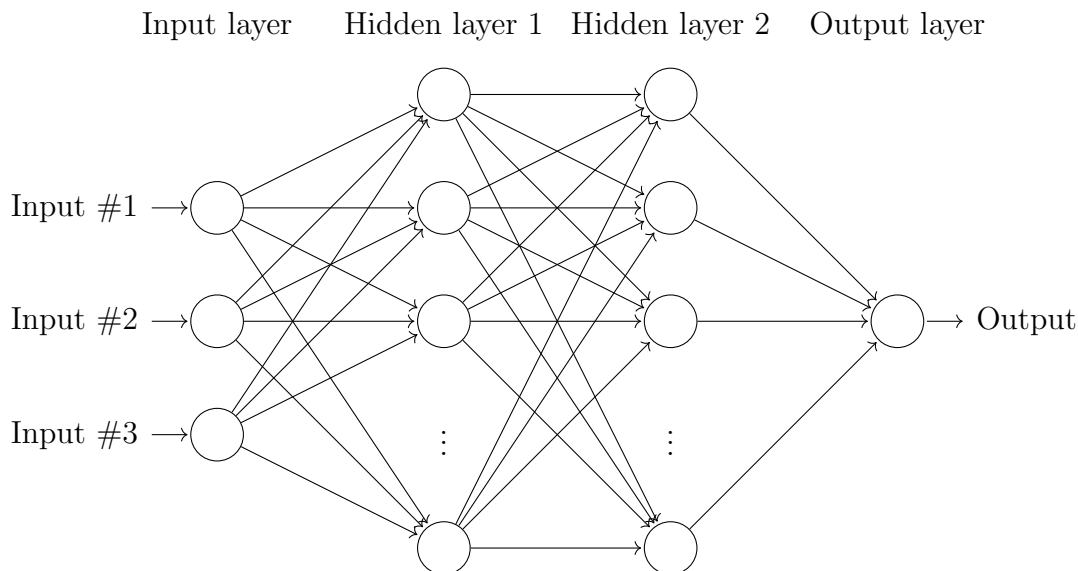


Figure 3-2.: Demonstration of a feed-forward neural network with structure of 3 inputs, 2 hidden layers, and 1 output.

In atmospheric science, especially for irradiance evaluation, more efforts of machine learning

have been put during the last decade of the past century (Elizondo *et al.* 1994; Mohandes *et al.* 1998; Gardner and Dorling 1998; Lopez *et al.* 2005; Khatib *et al.* 2012). Comparisons have been made between machine learning and Ångström–Prescott-type linear regression and other empirical models (Tymvios *et al.* 2005; Elminir *et al.* 2007; Jiang 2008; Kumar *et al.* 2015). One of the main drawbacks of machine learning approaches is that, as the ultimately determined weights of the network hardly reveal a specific physical relationship between inputs and outputs, an artificial neural network is just a black box, but even so, the merits are tempting. Our atmosphere is a complicated system, researchers have been crafting many empirical equations by trial and error for more than a century, and since this means is now handily available, we may let the artificial intelligence technique help us explore more interrelations among atmospheric variables.

The application of ANN is more an engineering way or even an art than a science (Chollet 2017). More details, along with programming language environment, choices of network structure and other hyperparameters, etc., will be unfolded in Chapter 5, along with a discussion of pros and cons of the three evaluation approaches.

4. Data

4.1. On the upper boundary condition

Before running any model, some boundary conditions are needed, such as: extraterrestrial irradiance, zenith angle of incident solar beam, daily maximum sunshine duration, etc.

Let us begin by assuming the Sun to be a blackbody, so it emits radiance according to Planck's function:

$$B_\lambda(T) = \frac{2hc^2}{\lambda^5(e^{hc/k_B\lambda T} - 1)}, \quad (4.1)$$

where h is the Planck constant, c is the speed of light, k_B is Boltzmann's constant, T is the temperature of the black body. We then have (cf. Eq. (2.2)):

$$Q_\lambda = \int_0^{2\pi} \int_0^\alpha B_\lambda(T) \cos \theta \sin \theta d\theta d\phi = \pi B_\lambda(T) \sin^2 \alpha = \pi B_\lambda(T) \frac{r_{sun}^2}{d_{sun-earth}^2}, \quad (4.2)$$

where α is the zenith half angle subtended by the Sun's disk. The Sun's radius is r_{sun} ; the Sun-Earth distance is denoted as $d_{sun-earth}$. Integrating with respect to wavelength, we get the irradiance at the TOA Q_\perp^\downarrow .

$$\begin{aligned} Q_\perp^\downarrow &= \int_0^\infty \pi B_\lambda(T) \frac{r_{sun}^2}{d_{sun-earth}^2} d\lambda \\ &= \frac{\pi r_{sun}^2}{d_{sun-earth}^2} \int_0^\infty B_\lambda(T_{sun}) d\lambda = \frac{\pi r_{sun}^2}{d_{sun-earth}^2} \cdot \frac{\sigma T_{sun}^4}{\pi} = \frac{\sigma T_{sun}^4 r_{sun}^2}{d_{sun-earth}^2}, \end{aligned} \quad (4.3)$$

where $\sigma = 5.67 \times 10^{-8} W/m^2 K^4$ is the Stefan-Boltzmann constant. If we insert the effective temperature of the Sun $T_{sun} = 5780 K$, the radius of the Sun $r_{sun} = 6.957 \times 10^8 m$ and the average distance between the Sun and the Earth $\bar{d}_{sun-earth} = 1.496 \times 10^{11} m$, we get the solar constant $Q_{const}^\downarrow = 1365.8 W/m^2$. Because the Sun-Earth's distance is not constant, Q_\perp^\downarrow varies along with the position of the Earth relative to the Sun; for instance, at perihelion, $d_{sun-earth} = 1.471 \times 10^{11} m$, and $Q_\perp^\downarrow = 1412.7 W/m^2$; at aphelion, $d_{sun-earth} = 1.521 \times 10^{11} m$, where $Q_\perp^\downarrow = 1321.3 W/m^2$.

From Eq. (4.3), we get the expression for extraterrestrial irradiance Q_0^\downarrow :

$$Q_0^\downarrow = Q_\perp^\downarrow \cos \theta = Q_{const}^\downarrow \left(\frac{\bar{d}_{sun-earth}}{d_{sun-earth}} \right)^2 \cos \theta, \quad (4.4)$$

where θ is the zenith angle, as introduced in Section 2.1, the angle between the normal vector of a horizontal surface and the solar beam. By denoting latitude as φ ; δ as solar declination, the angle between the plane of the equator and the solar beam, which varies from -23.45° to 23.45° due to the tilt of the Earth; and ω as hour angle, the angle between the local meridian and the meridian that includes the solar beam, which increases 15° every hour, due to the rotation of the Earth, we can write for the cosine of θ ,

$$\cos \theta = \cos \varphi \cos \delta \cos \omega + \sin \varphi \sin \delta. \quad (4.5)$$

To calculate $(\bar{d}_{sun-earth}/d_{sun-earth})^2$ in Eq. (4.4), we use the equation proposed by Spencer (1971), a truncated Fourier expansion, with a maximum error of 0.00001 (Iqbal 1983).

$$\begin{aligned} \left(\frac{\bar{d}_{sun-earth}}{d_{sun-earth}} \right)^2 &= 1.000110 + 0.034221 \cos \Gamma + 0.001280 \sin \Gamma \\ &\quad + 0.000719 \cos 2\Gamma + 0.000077 \sin(2\Gamma), \end{aligned} \quad (4.6)$$

where the “day angle” Γ is defined as,

$$\Gamma = 2\pi(d_n - 1)/365 \quad (4.7)$$

where d_n is the day number of the year.

In order to calculate the extraterrestrial irradiance and the daily maximum sunshine duration we largely use the code provided by Whiteman and Allwine (1986), who also present useful

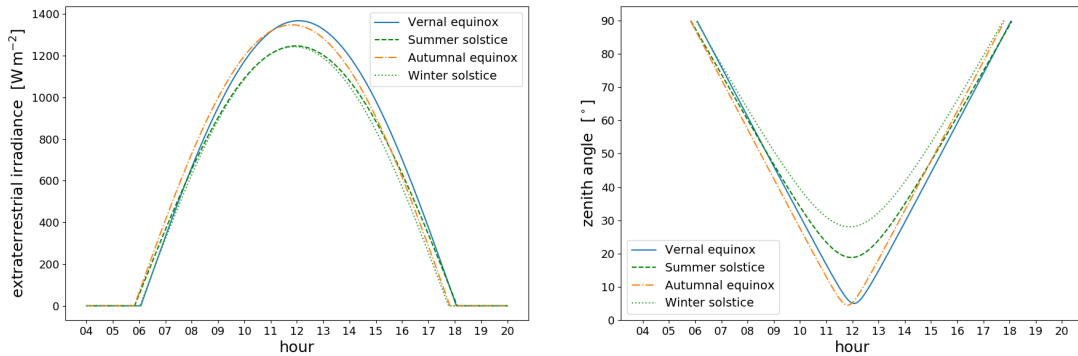


Figure 4-1.: Daily variations of extraterrestrial irradiance and solar zenith angle. The irradiance at the equinox days and the solstice days are shown. Figures calculated for the location of the station “EL IDEAM” (as for the choice of station, see more in the next section).

methods for calculating the hour angle ω , the declination δ , and the correction for the Local Standard Time (LST).

Fig. 4-1 shows how extraterrestrial irradiance and zenith angle vary during four representative days in a year. Fig. 4-2 shows how maximum daily sunshine duration and maximum daily irradiance change over a year, their variations are relatively quite small, owing to the close to the Equator latitude.

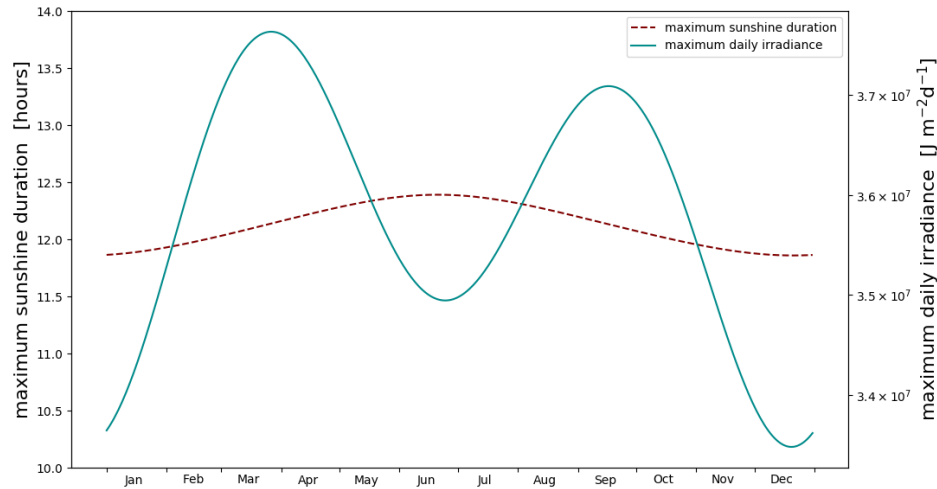


Figure 4-2.: Variations of maximum daily sunshine duration and maximum daily irradiance over a year, at the location of “EL IDEAM”.

4.2. Global irradiance data

The blueprint of our study is to apply three approaches—empirical regression, neural network and radiative transfer, using accessible variables to predict global irradiance at the surface. To evaluate results, we certainly need the data of the variable in question, namely, surface global irradiance, to compare the approaches with.

4.2.1. The station

The station “EL IDEAM” was chosen, for the following reasons:

1. Length of record. Two aspects were judged of importance: the completeness of the record, which means much less missing observations; and time span, which takes into account the length of the total record.
2. Quality of the data. Datasets are never perfect, and sometimes the quality of the data is unacceptable. Details of data validation of global irradiance measurements are presented in Appendix B.

3. Availability of other variables. We need other variables to estimate semi-empirically the global irradiance, so their availability was a factor in selecting the station.
4. Proximity. It was judged important to have access to the metadata of the selected station.

Taking these factors into account, the station “EL IDEAM”, with the geographic coordinate of $4^{\circ}36'28.8''\text{N}$, $74^{\circ}4'22.8''\text{W}$, stands out among the competitors. The instrument for irradiance measurement is a Kipp & Zonen CM11 pyranometer. Data is recorded every hour, with the unit W/m^2 , covering all significant spectrum of solar energy received at the Earth’s surface.



Figure 4-3.: Left: the pyranometer of the station “EL IDEAM”; Right: the author and the pyranometer.

4.2.2. From hourly measurements to daily values.

Measurements from the pyranometer are recorded hourly. To get daily average, we use Eq. (3.1), and because the measurements cover the whole frequency range, the integral over frequency need not be carried out. We multiply each hourly measurement by 3600, and sum them up to obtain daily values:

$$H_{daily} = \sum_{h=0}^{h=23} Q_h \cdot 3600 = \sum_{h=6}^{h=18} Q_h \cdot 3600. \quad (4.8)$$

On the left-hand side, the time limits are set at 06 : 00 and 18 : 00 indiscriminately, thanks to the fact that Bogotá is located near the equator line, so daily sunshine duration varies little over a whole year, and beyond these limits extraterrestrial irradiance is always zero.

We should notice that the hourly recorded data can not always truly represent the daily values. Fig. 4-4 draws the 2-minute recorded and hourly recorded data of the surface global irradiance in two days from the station “EL DORADO” (there are no 2-minute records on

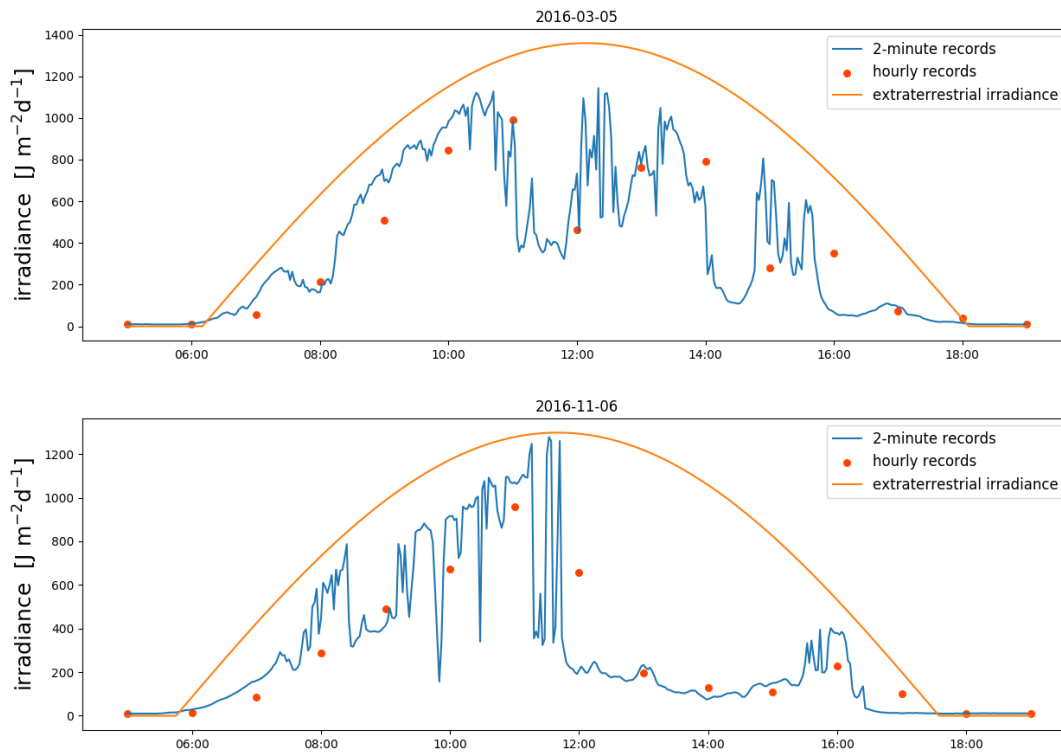


Figure 4-4.: The comparison between the 2-minute recorded data and the daily recorded data from the station “EL DORADO”, along with the extraterrestrial irradiance.

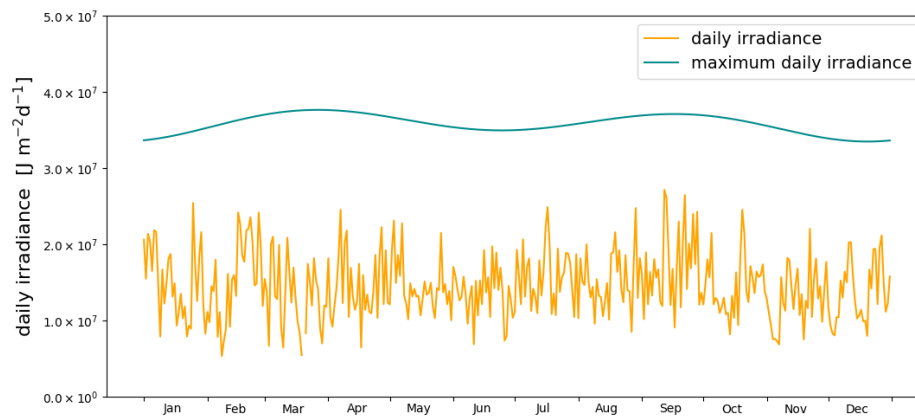


Figure 4-5.: The approximate daily irradiance and the calculated extraterrestrial daily irradiance over the year 2015, at the station “EL IDEAM”.

the station “EL IDEAM”), along with the extraterrestrial irradiance. It shows how surface global irradiance drastically varies during a day in Bogotá, and the fact that the hourly records do not always match with the 2-minute records. Fig. 4-5 shows the approximate daily surface global irradiance (from Eq. (4.8)) at “EL IDEAM” over a year, along with the extraterrestrial daily irradiance.

We might next define a *daily mean zenith angle* θ_d , which is needed by the program DISORT, to wit:

$$\theta_d = \frac{\int_{\text{sunrise}}^{\text{sunset}} \theta(t) \cdot Q_0^\downarrow(t) dt}{\int_{\text{sunrise}}^{\text{sunset}} Q_0^\downarrow(t) dt}, \quad (4.9)$$

the above equation can actually be viewed as a weighted arithmetic mean for daytime zenith angles, weighted by the corresponding extraterrestrial irradiance Q_0^\downarrow . Our calculation is done by numerical integration with an interval of one minute. A graph of θ_d changing over a year is shown by Fig. 4-6. By comparing Fig. 4-2 and Fig. 4-6 we can explain the bimodal shape of the maximum daily irradiance in Fig. 4-2, i.e., because of the change of the declination δ , or more directly, the change of the daily mean zenith angle θ_d .

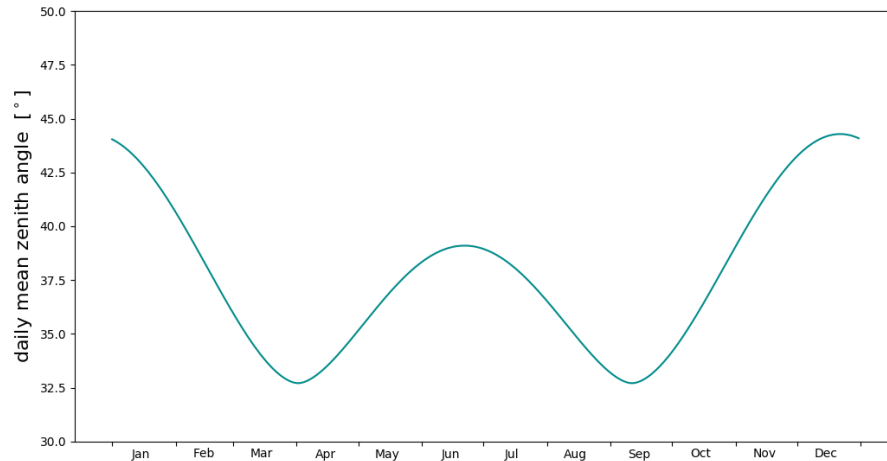


Figure 4-6.: Variation of daily mean zenith angle over a year, at the location of “EL IDEAM”.

4.3. Variables for predicting global irradiance

The traditional Ångström–Prescott model uses sunshine duration or cloudiness degree η to predict surface insolation. However there are no observations of them at the station “EL IDEAM”. To remedy this deficiency, we borrow sunshine duration data from 4 stations nearby, where Campbell–Stokes sunshine recorders are extant (Fig. 4-7). By means



Figure 4-7.: Locations of “EL IDEAM” (red) and nearby stations (blue) where equip sunshine recorders. Plotted in Google Map.

of an interpolation, we add weights to each station’s data depending on its distance to “EL IDEAM”. However, after many series of trials, equally weighted sunshine duration for all these 4 stations, actually provide better correlation with irradiance, so as a result simply the average values are applied. For cloudiness, only the surface synoptic observations (SYNOP) data from the international airport El Dorado include this information, but the distance between “EL IDEAM” and airport is around 12 km , and furthermore, observations are very subjective and limited in either values (octant numbers, from 1 to 8) or frequency of observations (recorded every 3 hours). Preliminary tests showed the correlation between the cloudiness degree information extracted from SYNOP and daily global irradiance was not such as to justify further efforts. Hence we will focus only on the sunshine duration.

As for machine learning, the necessary variables can be picked at our discretion. At “EL IDEAM”, hourly recorded data of temperature, humidity, pressure, precipitation are available and were adopted. Besides, precipitable water vapor data (column-integrated water vapor) obtained from permanent GPS stations, made available by the Servicio Geológico Colombiano was used. For more information on the methodology to obtain this variable, see Bevis *et al.* (1994). Like in the case of irradiance data, datasets of these variables are validated before use.

We also retrieved air quality data from the Secretaría Distrital de Ambiente, the indicator chosen being PM_{10} —particulate matter of size less than 10 micrometers in diameter. For the same reason as explained for the data of sunshine duration, we take the average of 11

stations in Bogotá's urban area.

4.4. Summary and size of dataset

To summarize the variables used, they are listed in Table 4-1. Amongst them is the extraterrestrial irradiance Q_0^\downarrow . From extraterrestrial daily irradiance H_0^\downarrow and daily irradiance H_g^\downarrow (H_0^\downarrow and H_g^\downarrow are obtained by Eq. (4.8)), we can get the clearness index k (defined by Eq. (3.3)). Relative sunshine duration σ is obtained by dividing the average of sunshine duration observations from 4 stations by the theoretical maximum daily sunshine duration. DoY is the day of a year. The remaining variables are hourly recorded data.

Table 4-1.: Summary of variables needed in this study.

Variable	Symbol	Measured unit	Frequency
Surface Global irradiance	Q_h	$W \cdot m^{-2}$	hourly
Extraterrestrial irradiance	Q_0^\downarrow	$W \cdot m^{-2}$	calculated
Surface daily irradiance	H_g^\downarrow	$J \cdot m^{-2} \cdot day^{-1}$	daily
Extraterrestrial daily irradiance	H_0^\downarrow	$J \cdot m^{-2} \cdot day^{-1}$	calculated
Clearness index	k	dimensionless	daily
Relative sunshine duration	σ	dimensionless	daily
Surface air temperature	T	$^\circ C$	hourly
Surface relative humidity	RH	dimensionless	hourly
Surface air pressure	P	hPa	hourly
Precipitable water vapor	PWV	$kg \cdot m^{-2}$	hourly
Precipitation	PT	mm	hourly
PM ₁₀	PM_{10}	$\mu g \cdot m^{-3}$	hourly
Day of year	DoY	dimensionless	daily

After validating and discarding invalid data for each variable, from the year 2008 to 2017, data from only 1381 days are left for analysis, or 37.8% percent of the ten-year time span. However, abundance of data is crucial for both empirical regression and ANN, we might try to prepare dataset separately due to the model applied, only considering the necessary

variable/variables in order to preserve more records for use, e.g., for the Ångström–Prescott-type regression, only sunshine duration σ and clearness index k are needed, then data from 1841 days are available; while for ANN, when σ is not used, data from 1692 days are available.

The probability distribution of these 1692 clearness indices k is shown in Fig. 4-8, with the sample mean equal to 0.35, and standard deviation equal to 0.11. A fitting of a Gamma distribution is also shown, with an approximate shape parameter 15.

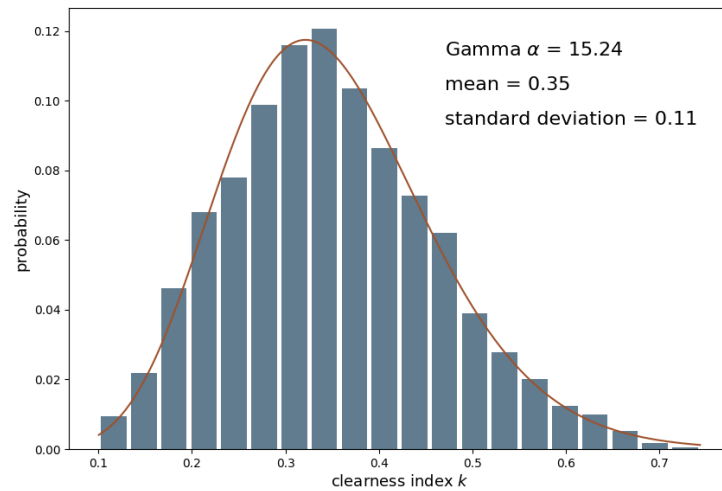


Figure 4-8.: Probability distribution of k , data grouped into 20 bins. A fitting line of a Gamma distribution is also shown, whose shape parameter is close to 15.

5. Experiments and results

5.1. Design of experiments

The idea of our numerical experiments is to make use of the datasets described in Chapter 4 to predict the clearness index k by three paths: radiative transfer, empirical regression, and ANN. These approaches seemingly share little similarity, whether from starting point or methods, but nevertheless, we shall make comparisons of several characteristics.

Table 5-1.: Comparison of three evaluation approaches in several perspectives. H, M, L are respectively short for high, medium and low, as attributes of criteria.

Method	Complexity	Model's Transparency	Flexibility	Variables demanded
RTE	H	H	L/H	H
Empirical	L	M	M	L
ANN	M	L	H	M

- **Complexity**
Radiative transfer has the highest complexity. Empirical approaches are used extensively because of their relative simplicity. The complexity of ANN depends upon its actual structure, but by and large it is more complex than empirical equations.
- **Transparency**
The black-box-like ANN makes it the least transparent. In RTE, on the other hand, details in the whole pathway of the light can be theoretically calculated at will, provided sufficient parameters and variables are accessible.
- **Flexibility**
We refer the flexibility here to two aspects: the flexibility of the choice of variable and the flexibility of model structure. From the viewpoint of the choice of variable, ANN can freely choose inputs, parameters needed for RTE are rather fixed; from the model structure's perspective, the choice of layer number in RTE and the choice of network architecture in ANN are both flexible.

- Variables required

The RTE would need many variables to calculate any quantity of the theory, so many that it is often not practical. In most cases, the empirical approaches have the lowest requirement of variables.

In our experiments, we supposed that the atmospheric constitution from the year 2008 to 2017 is time-independent. Although this is not the case in the real world, ten years, the time span of our data, is not a very long period, so climate characteristics could be considered as stable, instead of evolving in time, that is, *daily* variations of meteorological factors play the predominant role. The data can consequently be safely shuffled. All the regression coefficients and model scores will be obtained by averaging results from 30 repeated runs, and before each run, the dataset will be randomly shuffled.

Four metrics are used for evaluation of different models:

Pearson's r The Pearson correlation coefficient, or Pearson's r measures the linear correlation between two variables,

$$r(x, y) = \frac{\sum_{i=1}^n (x_i - \bar{x})(y_i - \bar{y})}{\sqrt{\sum_{i=1}^n (x_i - \bar{x})^2} \sqrt{\sum_{i=1}^n (y_i - \bar{y})^2}}. \quad (5.1)$$

We use Pearson's r to estimate the correlation between prediction and recorded data from the test set. In linear regression, however, this score has no difference with Pearson's r calculated from the two variables.

Mean absolute error Mean Absolute Error (MAE) estimates the average absolute difference between two variables with the expression:

$$MAE(x, y) = \frac{1}{n} \sum_{i=1}^n |y_i - x_i|. \quad (5.2)$$

We also apply MAE on prediction and recorded data from the test set, for its clear interpretation, and it is easy to compare the prediction departure with the magnitude of the physical quantity in question.

Mean bias error Mean Bias Error (MBE) measures the average of error bias. Since MBE does not take the absolute value, positive and negative errors cancel out, it gives the overall deviation to indicate whether a model is good at prediction in long period.

$$MBE(x, y) = \frac{1}{n} \sum_{i=1}^n (y_i - x_i). \quad (5.3)$$

Mean square error Mean Square Error (MSE) is the second moment of the error, we use it as the loss function in ANN to monitor the scores during the training process (see Section 5.3.1.2).

$$MSE(x, y) = \frac{1}{n} \sum_{i=1}^n (y_i - x_i)^2. \quad (5.4)$$

We start with the easiest applied empirical regression, followed by the neural network, and finally turn to DISORT.

5.2. Empirical regression

For empirical regression approaches, the data are separated into 75% for the training set, and 25% for the test set.

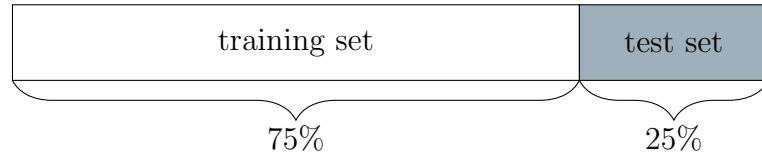


Figure 5-1.: Separation of dataset for regressions.

Linear regression for Ångström–Prescott equation (Eq. (3.3)) leads to:

$$k = 0.374 + 0.226 \cdot \sigma. \quad (5.5)$$

Quadratic regression leads to:

$$k = 0.225 + 0.379 \cdot \sigma - 0.008 \cdot \sigma^2. \quad (5.6)$$

Regression with Eq. (3.4) with respect to daily surface temperature range gives

$$k = 0.120 \cdot (T_{max} - T_{min})^{0.5}. \quad (5.7)$$

Scores of these three regressions (the test set) are shown in Table 5-2:

Table 5-2.: Scores of three empirical regressions.

	Pearson's r	MAE	MBE
Linear regression	0.6323	0.0683	-5.6×10^{-4}
Quadratic regression	0.6323	0.0686	-1.4×10^{-4}
Temperature range regression	0.4495	0.0805	-2.0×10^{-3}

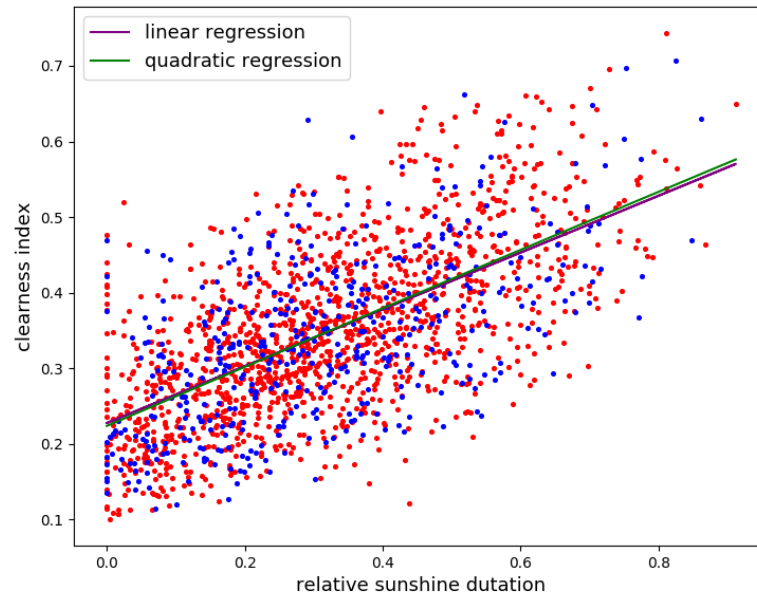


Figure 5-2.: Regression plot of relative sunshine duration σ and clearness index k . Red dots are training set, blue dots are test set, the purple line is the result of linear regression, the green line of quadratic regression. We can observe that these two lines are very close to each other.

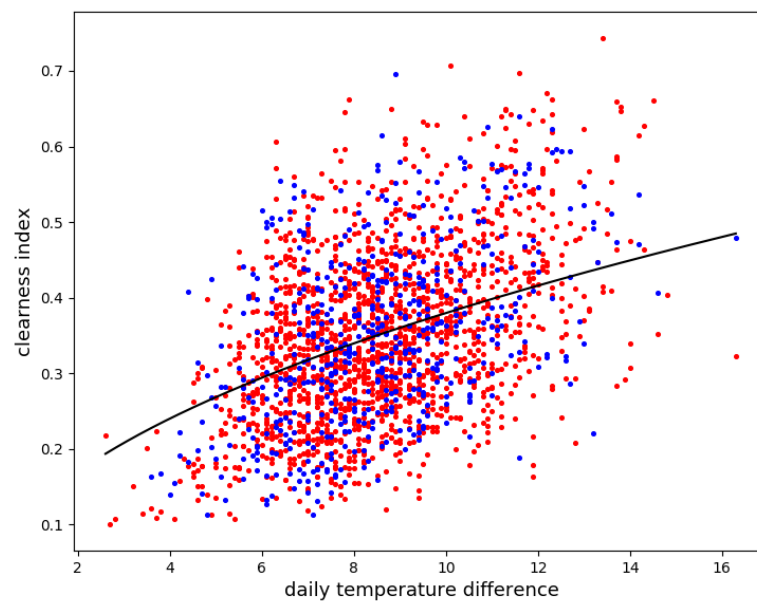


Figure 5-3.: Regression plot of daily temperature range and clearness index k . Red dots are training set, blue dots are test set, the black line is result of regression from Eq. (3.4).

Fig. 5-2 shows the data distribution of clearness index k and relative sunshine duration σ , along with the linear and the quadratic regressions; Fig. 5-3 shows data distribution of clearness index k and daily surface temperature range $T_{max} - T_{min}$, along with the regression of Eq. (5.7).

From Fig. 5-2 one can see that σ and k , though not tightly tied, show a degree of correlation. It also can be seen from both the scores and the figure that, a quadratic regression is unnecessary since performance is not improved, the small quadratic coefficient in Eq. (5.6) reflects this fact. On the other hand, the daily temperature range shows even less correlation with clearness index.

5.3. Artificial neural network

5.3.1. Architecture of neural networks

Neural networks in this thesis are built up by Keras, which is an open source Application Program Interface (API) based on Python. Keras is a high-level modular library, it relies on and runs on top of machine learning engines like “TensorFlow”, “Theano” or Microsoft cognitive Toolkit (“CNTK”). We use “Tensorflow”, a framework developed by Google, as the backend engine. Feed-forward neural network is chosen as the model type. Before training, we first determine the dataset structure and the hyperparameters.

5.3.1.1. Dataset for learning step

As Table 4-1 shows, most atmospheric variables that could be used as ANN’s inputs are recorded hourly, while the output k is daily values.

In the data science community, the structure of data, as far as their dimension number of variables is concerned, is usually distinguished by *tensors*. E.g., if an hourly recorded dataset contains 3 variables—temperature, relative humidity and air pressure, and grouped in days, then its structure is called a 2-Dimensional (2D) tensor with a (24,3) shape, where 24 refers to the recording times in a day, 3 refers to the three variables. A daily recorded dataset with 3 variables has a structure of a 1-Dimensional (1D) tensor, since there is no time dimension anymore. When just one daily variable is involved, the structure is further downgraded to a 0-Dimensional tensor, or a *scalar*.

We set the structure of hourly data—all of them are inputs—to a (11,n) 2D tensor. On most days in a year in Bogotá, the Sun rises around 6:00 and sets around 18:00, so atmospheric parameters at dawn or dusk contribute negligibly to the daily insolation, so we truncate the hour number to 11 (from 7:00 to 17:00); n, a flexible value, refers to the number of input variables.

We set the structure of daily data to a (1,n) 1D tensor, considering that daily variables such as relative sunshine duration and day of the year, could also be used as inputs. When only one input variable is dealt with, the structure downgrades to a scalar, which is also the case of the output, consisting only of one daily variable—clearness index k .

An extra step is needed to split the dataset as compared to the empirical regression method: a validation subset should be reserved from the training set to monitor the error, or the score, during the training process. 25% of the training set are held back for the *validation set* in this work. It is worth mentioning that the term validation here has a different meaning in the data science community as that mentioned in Chapter 4 or Appendix B. The process of examining and cleansing the faulty records is sometimes instead called *data scrubbing*, but without fear of ambiguity, the term “validation” will be kept. Moreover, *k-fold cross validation* is applied. We set $k = 4$, which means, the dataset other than the test set (75% in our work) is equally divided into 4 subsets, the model being trained 4 rounds, in each round one of these subsets will interchangeably be reserved as the validation set without repetition, while other 3 subsets are combined to still serve as the training set, as shown in Fig. 5-4. Finally, the test set, the same as in the regression method, is set completely aside as the unseen data.

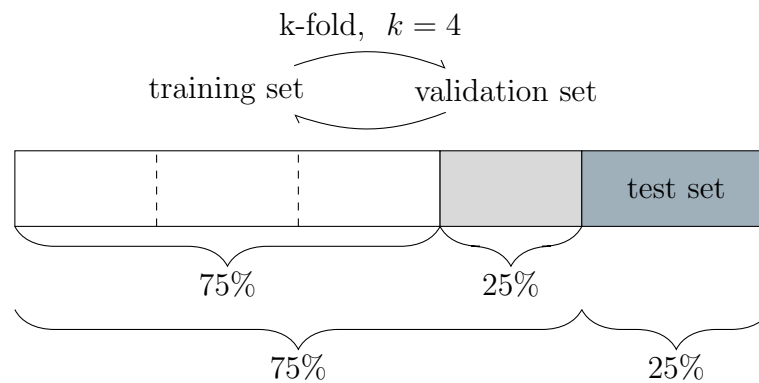


Figure 5-4.: Separation of dataset for neural network.

Another pretreatment is the *feature scaling* for inputs, as input variables have different scales or orders of magnitudes. It is important, often necessary, for an ANN model to rescale variables into a same range. One of the common techniques is standardization,

$$x' = \frac{x - \bar{x}}{\sigma}, \quad (5.8)$$

where x is the original value, \bar{x} and σ are the mean and the standard deviation of the training set. After the standardization, x' is used as the input.

5.3.1.2. Hyperparameters

Hyperparameters are parameters that should be set before the training phase. They include network structure, epoch number, batch size, activation function, loss function, optimizer, learning rate, regularization method, etc. In the following, these terms will be explained, along with our choice for each hyperparameter. It should be pointed out that, there are many possible configurations of hyperparameters for an ANN. The treatise by Géron (2017) could be referred to for many available options; however, only the hyperparameters eventually adopted will be presented below, which are singled out from a number of candidates by trial and error.

Neural network structure The structure of an ANN is composed of layer number, neuron number in each layer and the topology of neuron connections.

In the first and main case, inputs are hourly and $(11,n)$ 2D tensor data, while the output layer has the structure of a scalar. The network construction with $(11,3)$ 2D tensor inputs is shown in Fig. 5-5. To combine the 2D tensor input layer and the scalar output layer, we build 3 hidden layers, with respectively 12, 8 and 16 neurons in each layer. From the input layer to the second hidden layer, connections are hourly separated, which means that

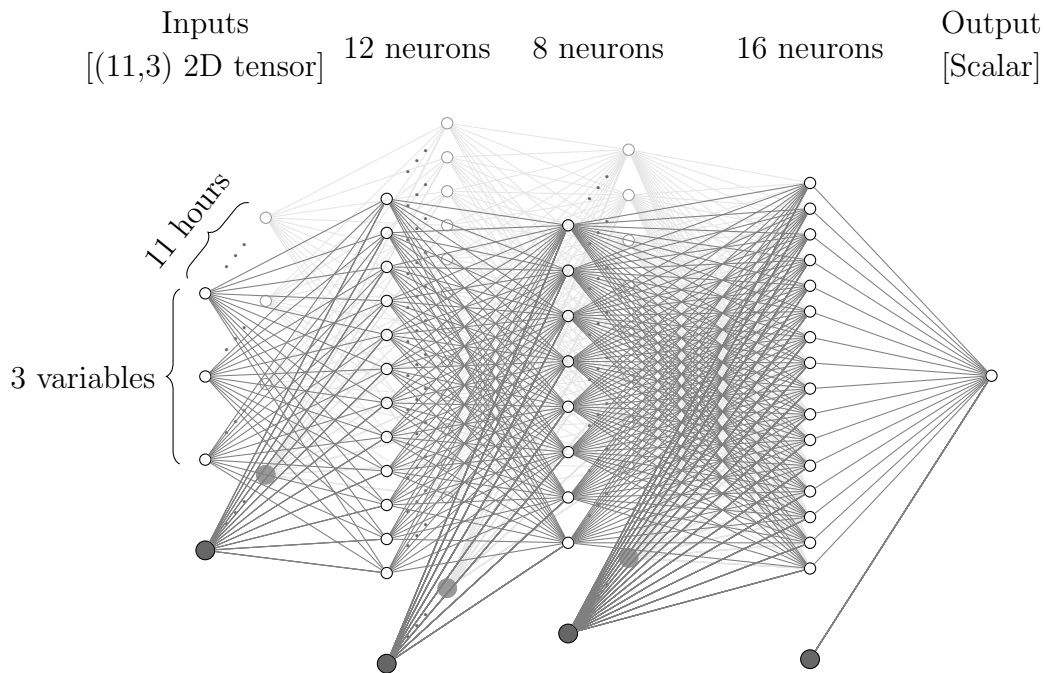


Figure 5-5.: Demonstration of a feed-forward neural network with 3 hidden layers. The structure of inputs is $(11,3)$ 2D tensor, the structure of output is scalar. Until the second hidden layer, neurons are hourly separately connected. Solid circles denote bias neurons.

within these three layers, neurons “belonging to one hour” do not have cross connections to neurons “belonging to other hours”. Then, the second hidden layer of (11,8) 2D tensor is fully connected to the third hidden layer of (16) 1D tensor (which means there are $11 \times 8 \times 16 = 1408$ connections and their weights between these two layers). Finally, all the neurons in the third hidden layer are connected to the scalar output layer. In addition, each layer, except the output layer has bias neuron/neurons, which, depicted as solid circles in Fig. 5-5, connect fully to the next layer. The purpose of bias neuron will be explained later with the configuration of “activation function”.

In the second case, daily inputs are also considered, as their structure is a 1D tensor or a scalar, they are placed at the same level as the 1D tensor third hidden layer, then fully connected to an additional fourth hidden layer with 5 neurons. This four-hidden-layer network construction is shown in Fig. 5-6.

Hourly inputs 12 neurons 8 neurons 16 neurons 5 neurons Output

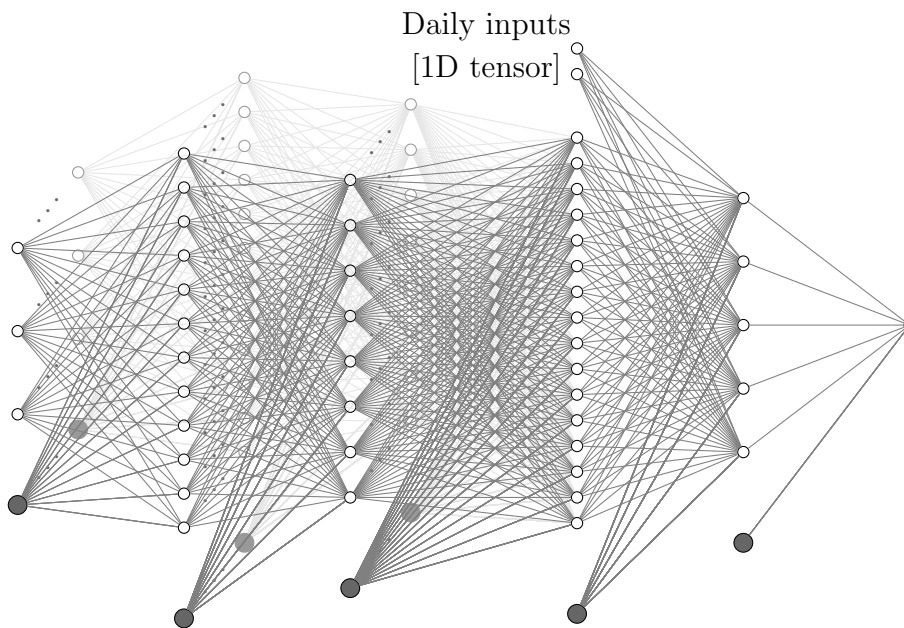


Figure 5-6.: Demonstration of a feed-forward neural network with 4 hidden layers. Besides the hourly (11,3) 2D tensor inputs, there are also daily (2) 1D tensor inputs. One extra hidden layer is added to the construction in Fig. 5-5 before connecting to the output layer.

Epoch number One epoch is defined when the ANN algorithm runs through the whole training set. Though we set the epoch number at 1000, usually however the training process will not reach the 1000th epoch (see *early stopping* below).

Batch size The batch size is the number of training samples that are passed through the network at one time when all the weights are updated once, so the model tends to learn faster with a higher batch size setting. The setting depends on the computer memory and capability. We set batch size 16.

Activation function The activation function of a neuron converts input signals from the previous layer to an output signal of this neuron, it builds a non-linear connection between layers and eventually between inputs and outputs of the network. An activation function should be differentiable for back-propagation to be possible. We finally chose a *sigmoid*, which is a logistic function (Hagan *et al.* 2014):

$$S(x) = \frac{1}{1 + e^{-x}}, \quad (5.9)$$

then the output of neuron j in layer i is:

$$O_{ji} = S\left(\sum (W_{kj} \cdot O_k) + bias\right), \quad (5.10)$$

where k indicates the index of a neuron in layer $i - 1$, O_k represent the outputs (activations) from neurons in layer $i - 1$, W_{kj} are connection weights between layer $i - 1$ and layer i . The bias neurons, shown by solid circles in Fig. 5-5 and Fig. 5-6, serve to shift the whole weighted sum, it being analogous to the constant or the intercept term in a polynomial regression.

Loss function Loss function is the function that measures the error of predictions with respect to the recorded data. To improve the performance of an ANN simply means to minimize its loss function. We use MSE as the loss function.

Optimizer Optimizer is the actual algorithm to improve the performance. It specifies how a network optimizes by self-modifying its weights. In a feed-forward neural network, this is done by back-propagation. Starting with the loss function, the algorithm propagates backward through the network carrying the error information to update the weights. *Gradient descent* is the core technique to do this. We choose *Adam*, which belongs to a group called adaptive learning algorithms, whose learning rate is adapted for each parameter (Ruder 2016).

Learning rate It defines the pace at which weights will be updated by the optimizer in back-propagation. While for a higher learning rate the model will learn faster, it may not be able to reach the lowest value of the loss function; at lower learning rates, the model will adjust more carefully each time, but may not be able to escape from a local minimum to reach a global one. We set the initial learning rate for Adam optimizer at 0.0002.

Regularization This is a technique to prevent overfitting, which means the model fits too well on the training set that it fails to generalize to the unseen dataset. Regularization methods include penalizing the large weights, randomly *dropping out* (setting to zero) a portion of activations of a layer, etc (Chollet 2017). However, we chose not to use regularization.

Early stopping Early stopping could also be regarded to be part of the regularization technique, except it applies to time. The loss function is calculated on both training and validation set. To avoid overfitting, the training process will be stopped when the loss function of the training set has been consecutively lower than that of validation set in a number of epochs. We set the *patience* of early stopping in Keras equal to 40.

Our networks are built based on the 9 hyperparameters discussed above.

5.3.2. Input variables and performances

Theoretically, all independent variables in Table 4-1 have an influence to some extent upon the output, clearness index k . However carrying out all the combinations of those variables is not necessary. E.g., we have 9 input variable candidates, so there will be $2^9 = 512$ combinations if applying the exhaustive searching method. In data science, the process of choosing a subset of relevant variables is called *feature selection*. To do that, we conduct experiments on a subset of input combinations based on physical understanding, and a number of additional experiments will also be done as control groups for comparison. 9 input variable candidates and the results of 32 experiments are listed in Table 5-3, the respectively chosen variables being shown as gray boxes. The first 7 variables (Q_0^\downarrow , T , RH , P , PWV , PM_{10} , PT) in the Table are hourly variables. If only these variables are used, the ANN structure of Fig. 5-5 applies, but if any daily variable (σ , DoY) is combined to make up the input, the structure of Fig. 5-6 applies.

Another strategy was also tried, which is, setting hourly irradiance values Q_h as outputs, instead of the daily clearness index k , we then compute k afterwards by applying Eq. (4.8). Nevertheless, the results do not show significant differences with respect to models that set k as the output, so this scheme will not be exhibited or discussed.

The dataset is shuffled before running every model, each model is run 30 times and their average scores are presented. We can see that the results with highest scores among these experiments share Pearson's r around 0.8, and MAE around 0.054. By observing Table 5-3, all the models of the 11 highest scores include input variable Q_0^\downarrow , RH and PM_{10} , thus, the Q_0^\downarrow - RH - PM_{10} input combination is considered to be the optimum (these three variables are also depicted by darker color in all lines of Table 5-3). Even though the combination exactly of these three variables is the one that holds the fourth highest score, we should be aware of that, first, the superiorities of three higher scores are not significant; second, the sample do not represent the whole population; third, the shuffling procedure of dataset also introduces

Table 5-3.: ANN scores from 32 experiments (ranked by Pearson’s r). Input variables in each experiments are shown as gray boxes. 3 variables— Q_0^\downarrow , RH and PM_{10} , whose combination is believed to be the optimum one, are highlighted by darker color.

Experiment	Inputs									Metrics of models		
	Q_0^\downarrow	T	RH	P	PWV	PM_{10}	PT	σ	DoY	Pearson’s r	MAE	MBE
1	Dark	Light	Dark		Light	Dark				0.8006	0.0541	1.7×10^3
2	Dark		Dark		Light	Dark				0.8000	0.0536	1.7×10^3
3	Dark		Dark	Light	Light	Dark				0.7992	0.0538	2.2×10^4
4	Dark		Dark			Dark				0.7985	0.0537	3.4×10^4
5	Dark		Dark			Dark		Light		0.7983	0.0537	1.2×10^3
6	Dark	Light	Dark			Dark				0.7964	0.0537	-5.5×10^4
7	Dark	Light	Dark			Dark	Light			0.7944	0.0537	-4.6×10^4
8	Dark	Light	Dark	Light		Dark				0.7939	0.0538	-3.0×10^4
9	Dark		Dark	Light		Dark		Light		0.7923	0.0547	-8.2×10^4
10	Dark		Dark			Dark	Light			0.7907	0.0543	-8.4×10^4
11	Dark		Dark	Light		Dark				0.7902	0.0542	-3.5×10^3
12		Light	Dark	Light		Dark				0.7869	0.0543	2.4×10^3
13			Dark			Dark		Light	Light	0.7843	0.0546	5.5×10^4
14			Dark	Light	Light	Dark				0.7832	0.0555	1.7×10^3
15			Dark	Light		Dark	Light			0.7815	0.0557	3.2×10^3
16			Dark		Light	Dark				0.7760	0.0558	2.5×10^3
17			Dark			Dark				0.7724	0.0557	-2.2×10^3
18		Light	Dark			Dark				0.7721	0.0559	-7.1×10^5
19	Dark		Dark			Dark			Light	0.7717	0.0563	2.5×10^3
20	Dark		Dark			Dark				0.7710	0.0565	-8.2×10^4
21			Dark	Light	Light	Dark				0.7702	0.0562	9.8×10^4
22			Dark	Light		Dark				0.7654	0.0566	2.2×10^5
23	Dark		Dark	Light		Dark		Light	Light	0.7646	0.0562	-1.0×10^3
24		Light	Dark	Light	Light	Dark				0.7578	0.0572	1.2×10^3
25		Light	Dark			Dark				0.7468	0.0590	3.3×10^3
26			Dark			Dark				0.7361	0.0591	1.9×10^3
27			Dark			Dark			Light	0.7202	0.0597	5.6×10^4
28	Dark	Light				Dark				0.7024	0.0632	-1.8×10^3
29		Light		Light		Dark				0.7022	0.0633	3.4×10^3
30	Dark				Light	Dark				0.6313	0.0696	-3.0×10^3
31					Light	Dark				0.6240	0.0707	-2.9×10^3
32	Dark				Light	Dark				0.5969	0.0725	-9.5×10^4

randomness. According to “Occam’s razor principle”, we choose the simpler inputs. Any other combinations including Q_0^\downarrow - RH - PM_{10} (line 1, 2, 3, 5, 6, 7, 8, 9, 10, 11, 19 and 23) do not produce significantly, if any, better outcomes; combinations with variables less than 3 degrade the scores severely (line 17, 20, 22, 25, 26, 31 and 32); the rest of the combinations (line 12, 13, 14, 15, 16, 18, 21, 24, 27, 28, 29 and 30) do not generate better results either.

From Table 5-3, the conclusion in the previous section is supported, namely, that temperature range is not an appropriate variable to estimate surface insolation.

By contrast, attention should be drawn to the fact that, the surface relative humidity RH by itself (line 26) already yields an acceptable score, which exceeds that of traditional regressions (Table 5-2). We thus might try linear and quadratic regressions for RH and k by the same procedure as in Section 5.2. A similar technique as Eq. (4.9) is applied to generate a *daily average relative humidity* RH_d :

$$RH_d = \frac{\sum RH(h) \cdot Q_0^\downarrow(h)}{\sum Q_0^\downarrow(h)}. \quad (5.11)$$

Regression results, data scatter and scores are shown in Eq. (5.12), Eq. (5.13), Fig. 5-7 and Table 5-4. It can be seen that even the linear regression of RH_d and k has outdone the Ångström–Prescott regression, either by producing higher regression scores or in view of the more tightly clustered distribution of data.

$$k = -9.77 \times 10^{-3} + 0.924 \cdot RH_d, \quad (5.12)$$

$$k = 1.230 - 2.02 \times 10^{-2} \cdot RH_d + 8.75 \times 10^{-5} \cdot RH_d^2, \quad (5.13)$$

Table 5-4.: Scores of regressions between daily average relative humidity RH_d and clearness index k .

	Pearson’s r	MAE	MBE
Linear regression	-0.7198	0.0611	6.4×10^{-4}
Quadratic regression	-0.7247	0.0605	-6.8×10^{-4}

We look for reasons of why the best inputs were found to be Q_0^\downarrow - RH - PM_{10} instead of others.

First, it is conceivable that PM_{10} , representing the air quality, contributes to the optical depth; second, RH is a relative value, it does not only include information of the water vapor, it includes information of atmosphere’s temperature as well, which is also related to solar radiation; third, there is another possible reason that RH predicts better than T , that T reacts quickly with the environment, a cumulus cloud coming and going could cause

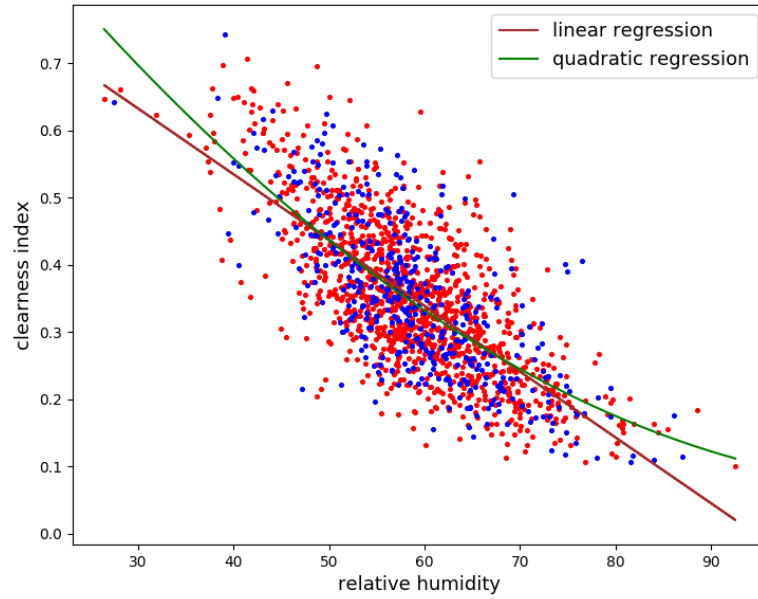


Figure 5-7.: Scatter diagram of daily average relative humidity RH_d and clearness index k . Red dots are training set, blue dots are test set, purple line is the result of linear regression, green line that for quadratic regression.

fluctuation of the surface temperature, and as the hourly measurement of T is recorded only at one moment, it might not truly reflect the average temperature of that particular hour. RH on the other hand, changes more smoothly, thus it more closely represents the average values of an hour.

Surface air pressure P cannot be viewed as an indicator of weather in Bogotá, since pressure is not relevant here.

Precipitable water content PWV could provide information about cloudiness, which partly may already be contained in the surface relative humidity RH .

As to DoY , if the daily irradiance values over a year show any patterns, the extraterrestrial irradiance Q_0^\downarrow should reflect this information. From Fig. 4-5, we can also see that the daily irradiance does not have a clear pattern over a year.

While for the precipitation PT , it does not necessarily indicate cloud amount, a non-precipitable cloud may subsist a long time to block the sunshine.

Above all, regarding clearness index k , based on feature selection and physical analysis, Q_0^\downarrow , RH and PM_{10} are the most relevant variables; RH , PWV , T and DoY might be considered as redundant variables; P and PT might be considered as relatively irrelevant variables.

5.4. Radiative transfer method

5.4.1. Feature of irradiance in tri-layered model

For radiative transfer calculations, the DISORT code (version 4.0.98) and the tri-layered model introduced in Section 2.4 are used. In all computations, we chose an 8-stream approximation, which takes both accuracy and computing speed into account. One caveat should be stated: the direct result from RTE is radiation or irradiance. We use DISORT to obtain daily energy by defining some effective parameters, such as daily mean zenith angle, daily effective optical depth, etc. If we let $H_0^\downarrow \equiv 1$, calculating k and H_g^\downarrow are equivalent.

Although the tri-layered model is a “minimal” model, still various parameters are needed, Table 5-5 shows our settings of phase function $P(\cos \Theta)$, optical depth τ and single scattering albedo $\tilde{\omega}$ for each layer, the daily mean zenith angle θ_d being calculated by Eq. (4.9), and the surface albedo ρ_L is set to be 0.15. The optical depths of middle layer τ_m and lower layer τ_l are left unfixed, for these two parameters change most drastically in time. Their values could serve to represent daily features.

Table 5-5.: Parameterization for the tri-layered model, all values are for daily calculations.

	$P(\cos \Theta)$	τ	$\tilde{\omega}$	θ_d	ρ_L
upper layer	isotropy	0.02	0.97	Eq. (4.9)	0.15
middle layer	HG with $g = 0.85$		0.95		
lower layer	HG with $g = 0.70$		0.8		

We now examine some daily radiative features under several typical atmospheric conditions, which is shown in Fig. 5-8. Each diagram divides the upper layer, the middle layer and the lower layer from left to right, with both direct and diffuse part of irradiance drawn, as well as their sum—the global irradiance. We also call the diffuse radiation *skylight*. The abscissa represents optical depth, while it is re-scaled to make each layer occupy a fixed length in the scheme. The ordinate is the clearness index k . The only parameters changed in these four cases are two optical depths: τ_m and τ_l , the others being set as in Table 5-5. The four scenarios are: clear day: $\tau_m = 0.64, \tau_l = 0.3$; cloudy day: $\tau_m = 9.0, \tau_l = 0.4$; polluted day: $\tau_m = 1.0, \tau_l = 1.0$; a presumably normal case: $\tau_m = 5.0, \tau_l = 0.5$. Note that in the clear day example, even if the air density is much thinner above the boundary layer than below, we still set τ_m more than twice than τ_l , due to the fact that, in the tropics, the height of the lower layer is much smaller than the middle layer, for the troposphere can reach up as high as 20 km. The zenith angle is set to 40°, which is a typical daily mean zenith angle in Bogotá (cf. Fig. 4-6). The optical depth where the skylight reaches its maximum is indicated by the green dashed line. Interestingly, in a clear sky condition ($k = 0.80$), skylight would never

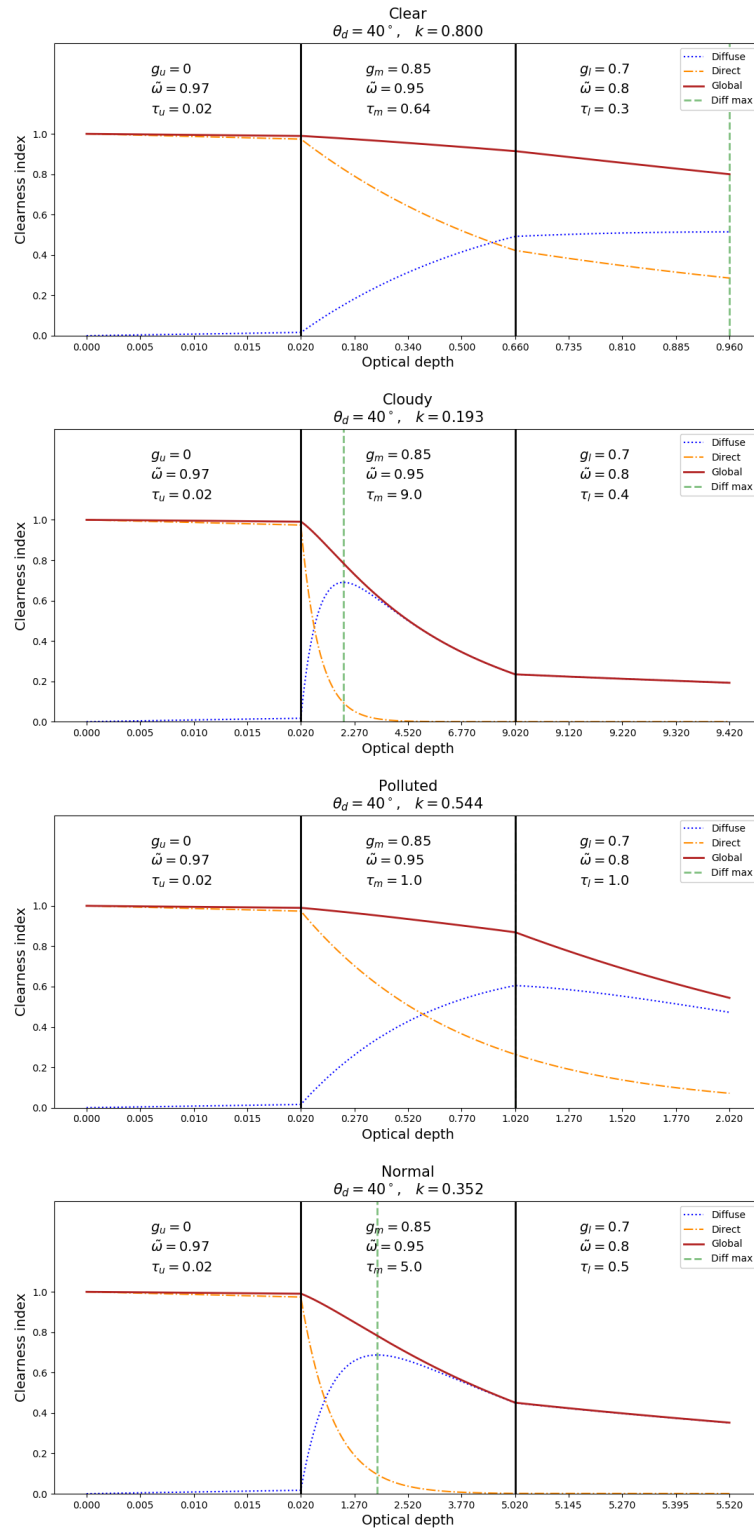


Figure 5-8.: Radiative features under four scenarios: clear day, cloudy day, polluted day and normal day. The vertical green dash line indicates the optical depth where diffuse irradiance reaches its maximum.

peak before it touches the ground; in the other cases, this peak will occur in the middle layer, except in the polluted-day scenario, where skylight reaches its maximum at the boundary between the middle and the lower layer (third panel in Fig. 5-8).

A phenomenon that might be found counter-intuitive from our everyday experience is that, even in a clear day condition (first panel in Fig. 5-8), the direct irradiance has quite a low value when it reaches the surface. From the shadow on the ground in any sunny day, we might claim a higher value. With the condition of forward-peak phase functions ($g_m = 0.85$ and $g_l = 0.70$ in Henyey-Greenstein approximation) and shallow optical depth, and even if the solar beam is scattered, it still has a forward component and concentrates closely around the original path, but it actually belongs to the diffuse part in the calculation, people on the ground could still experience it as the direct part.

5.4.2. Prediction by DISORT

In the previous model, the prediction of daily clearness index k is reduced to the estimation of τ_m and τ_l .

Optical depth in the lower layer τ_l As we discussed in Section 2.4, the lower layer is characterized by water vapor and aerosols. However, the variability of aerosol load is more pronounced and modifies significantly the optical depth, and we would like to simplify its determination by extracting information about the τ_l of aerosols. There is global aerosol optical depth (AOD) data available, such as from the Moderate Resolution Imaging Spectroradiometer (MODIS) of NASA, but it is subject to the limitations of both spatial resolution (1° , or 111 kilometers) and time resolution (data provided by polar orbit satellites). We therefore turn to locally recorded data of PM_{10} . Research on the relationship between PM_{10} and AOD (at 0.55 microns) at Bogotá has been done by Guevara Luna *et al.* (2018), who give a linear regression, but with a negative intercept (or constant term), see Eq. (5.14). Because a negative value of AOD is not acceptable, we offer a linear regression without an intercept, see expression Eq. (5.15) below, and whose graph is shown in Fig. 5-9.

$$AOD = 0.0209 \cdot PM_{10} - 0.953, \quad (5.14)$$

$$AOD = 0.00472 \cdot PM_{10}. \quad (5.15)$$

At first sight, Fig. 5-9 does not exhibit a strong correlation, we see that Pearson's r between these two samples is only 0.44, but by looking at Eq. (2.5), ρ and τ do have a linear relationship; also notice the fact that the sampling of these two variables cannot possibly match well with respect to time or location, so we keep the idea of a linear regression.

To represent τ_l with the help of AOD, there is more work to do. The AOD values we use are solely measured at the wavelength of 0.55 microns, but definitely there are more constituents

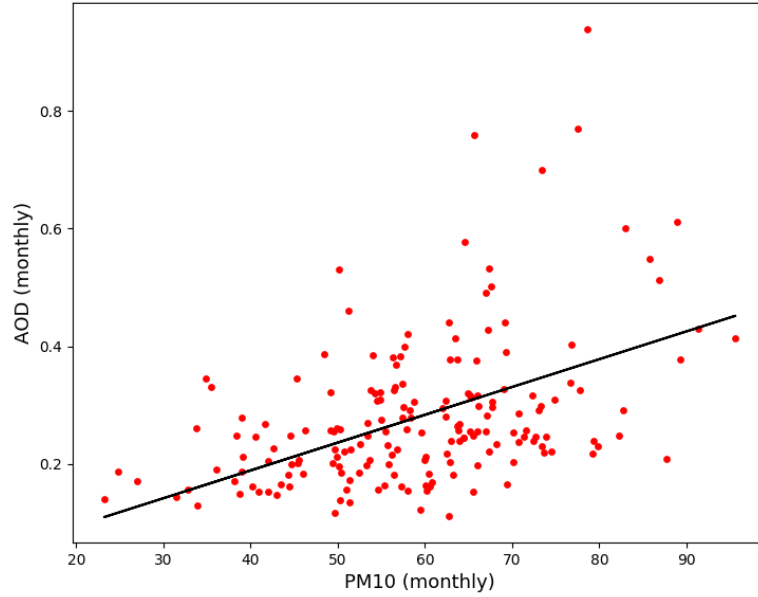


Figure 5-9.: Linear regression between monthly AOD and PM_{10} from 2001 to 2015. (The collection of data is courtesy of Guevara Luna *et al.* (2018))

in the lower atmosphere that will contribute to the optical depth. Therefore, we construct a modified empirical expression, adding a coefficient 1.4 and a constant term 0.25 for the representation of τ_l :

$$\tau_l = 1.4 \cdot AOD + 0.25 = 0.0066 \cdot PM_{10} + 0.25. \quad (5.16)$$

Optical depth of the middle layer τ_m An average daily value for τ_m is largely related to the cloudiness degree, whose information, unfortunately, is hard to retrieve directly (as discussed in Section 4.3). We turn our eyes to ANN. As we know from Section 5.3.2, the variables that provide most information to global irradiance are extraterrestrial irradiance Q_0^\downarrow , surface relative humidity RH , and an air pollution index PM_{10} , but of these, in our tri-layer model, PM_{10} is related more to the lower layer, so we use Eq. (5.16) to evaluate the τ_l , and so there are two variables left, Q_0^\downarrow and RH to predict τ_m . The structure of this hybrid model is shown below in Fig. 5-10:

The score from this hybrid model is shown in Table 5-6. We can see that whilst the MAE score is unable to compete with most scores from ANN, the Pearson's r on the other hand is acceptable. Fig. 5-11 shows the probability distributions of τ_l and τ_m from our particular determination. It makes sense that the shape of probability distribution of τ_m is closer to k than τ_l is (see Fig. 4-8), for τ_m does have a greater weight in radiative transmission through the three layers.

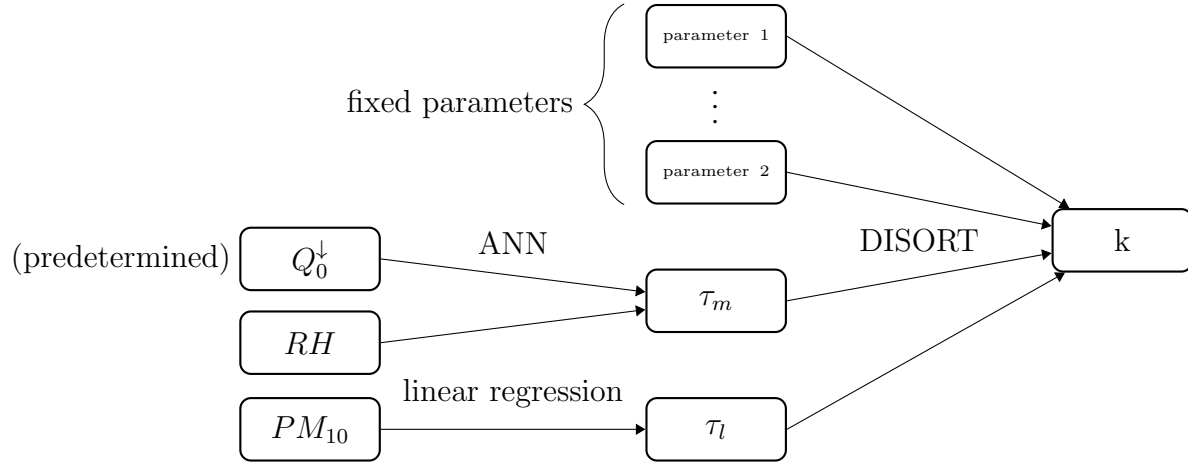


Figure 5-10.: A hybrid model that uses ANN, linear regression and DISORT to predict the clearness index.

Table 5-6.: Three-score metric of the hybrid model.

	Pearson's r	MAE	MBE
Hybrid model	0.7613	0.0625	-1.6×10^{-2}

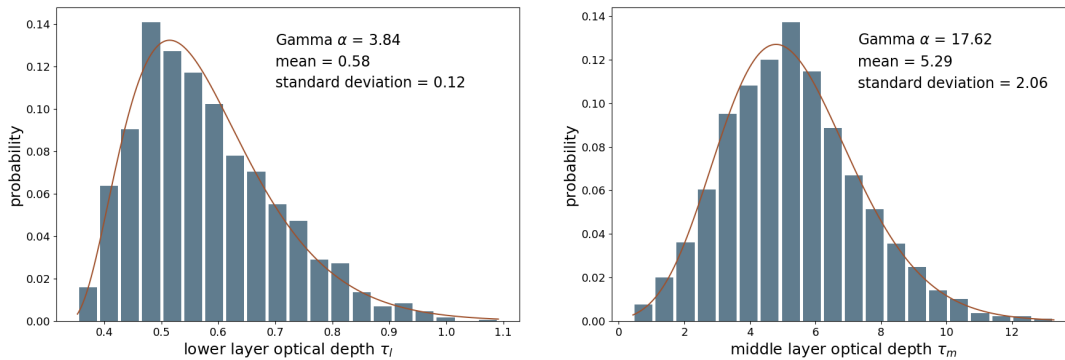


Figure 5-11.: Probability distributions of optical depths in the lower and the middle layers, each data are grouped into 20 bins.

6. Conclusions

So far in this work, theoretical studies along with numerical exercises have been carried out by three different methods. A complementary table to echo the comparisons at the beginning of Chapter 5 is shown below.

Table 6-1.: Comparison of evaluation approaches from several perspectives. H, M, L are respectively short for high, medium and low.

Method	Accuracy in theory	Accuracy with accessible variables
RTE	H	M
Empirical	M	L
ANN	unpredictable	H

An overview of our results shows that, the mean bias errors in the three approaches are all low (high scores), meaning that they qualify for long-term prediction; with other model scores, artificial neural network has the better performance, in comparison with the other two approaches.

First let us look at the empirical regression approach, whose performance is lowest. This long-standing empirical approach has its physical justification, of course. For example, the ground-based sunshine duration records relate to the total energy amount received on the surface. There are, however, problems with the approach: 1) we did not use data of sunshine duration and irradiance from the same location, and the “borrowed” sunshine data from surrounding stations cannot avoid the “inconsistency” of weather conditions, particularly considering the complicated weather system in the plateau of Bogotá; 2) sunshine duration given by Campbell-Stokes recorder does not weigh the values with extraterrestrial irradiance at a given moment, a burnt mark on a card at late afternoon will not distinguish from high noon, or say, a heavily burnt mark and a mildly burnt mark contribute indiscriminately to the observation, while the insolation at each relative moment is unlikely to be the same; 3) human factors cannot be ignored, e.g. reading values on a card is after all a subjective process, different observers might read out different results from the same card. There are many more empirical regression approaches based on all types of variables, and researchers

have devised a variety of forms with different coefficients. However, coefficients can, and should be related to the actual atmospheric parameters (Pelkowski 2009), which vary from one place to another.

Next we consider the neural network approach, which produced higher prediction scores compared with the other two approaches in our work. Machine learning has attracted more and more attention either in data science or meteorology. Where many authors build artificial neural networks trying to get better irradiance prediction, we take it one step further, using feature selection to find out the most relevant input variables, where a heuristic method was chosen to decide and limit the input variable candidates. The Q_0^\downarrow - RH - PM_{10} inputs (extraterrestrial irradiance, surface relative humidity, and surface pollution index PM_{10}) turn out to be the optimum among all others. This result makes sense, as: 1) the relative humidity is most related to the cloud system, which exerts most influence on the optical depth; 2) the pollution also significantly affects the atmosphere’s transparency; 3) finally, the pre-calculated extraterrestrial irradiance provides information of hourly weights. While other variables might as well be relevant to clearness index k , they are redundant to the Q_0^\downarrow - RH - PM_{10} combination, and thus by “Occam’s razor rule” we take as few input variables as possible.

Finally let us take the radiative transfer approach. The specific solution we chose is the discrete ordinate with the aid of a widely used programming code—DISORT. We simplify our atmosphere to a medium that contains only three layers, whose imagined borderlines are the tropopause and the top of the atmosphere’s boundary layer. For the aim of daily value calculations, concepts like effective daily optical depth and daily mean zenith angle are introduced, and other rather stable parameters are hypothesized by meteorological reasoning. We still need assumptions to parameterize τ_l and τ_m : based on the idea of the tri-layered model and analysis from the previously applied artificial neural network model, PM_{10} was chosen to estimate τ_l by linear regression, RH and Q_0^\downarrow were chosen to estimate τ_m by artificial neural network modeling. Despite all this, the score of this hybrid model is not impressive—better than empirical regression, yet behind the artificial neural network. We surmise some reasons for it: 1) the linear regression for τ_l loses too much information, the low Pearson’s r also shows the imperfection of this makeshift; 2) our parameterization method for the tri-layered model oversimplifies our complicated atmosphere; 3) variables do not separately contribute to the optical depths of the lower and the middle layers. E.g., high surface relative humidity could affect the optical depth in the lower layer; in turn, the aerosols might facilitate the nucleation activity in condensation and the cloud formation in the middle layer.

We close with some practical suggestions, along with recommendations for future work.

As far as applications are concerned, the fact should be noticed that the manually operated sunshine recorder is not able to continuously provide highly reliable data; on the other hand, we have found that a single surface relative humidity variable RH (we actually applied

another variable—extraterrestrial irradiance Q_0^\downarrow for hourly weighting, but it is calculable beforehand) can predict the daily irradiance better than sunshine duration does. (By the way, humidity sensors are normally more economical, and more reliable, with less human manipulation required). Therefore, the RH data could also be employed for the irradiance prediction. For this country, nevertheless, as our experiments were all limited to one station, the regression does not represent general conditions due to the complicated and special topography. To verify and validate our conclusion above, data from other and more diverse areas will be needed to test them in future work; a station at which both sunshine recorder and pyranometer are present would be a better choice to make comparison of the three prediction approaches. If an artificial neural network is applied to multiple stations, variables like latitude and elevation should then be considered as inputs.

In regard to the radiative transfer theory, while the radiative transfer approach is not tractable for the purpose of surface insolation estimation, we still put a lot of effort into studying that theory. It falls short of an easy-to-implement method, from the pragmatic viewpoint, but it is nonetheless the only means to understand the atmospheric radiation behavior.

As recommendation for future work, a more elaborate method of parameterization could be tried; second, since our method for deciding τ_l and τ_m was rather coarse, the hybrid model could have lost some capacity to evaluate proper values. There is another possibility: let a machine or a neural network itself learn the combination of daily τ_l and τ_m . One possible approach is to set outputs of the original neural network as τ_l and τ_m , instead of k , but τ_l and τ_m do not have observations to compare with. A possible remedy could be to attach the DISORT program to the end of the neural network, letting DISORT be the last layer, and using numeric methods to rewrite the back-propagation algorithm for this “DISORT” layer. This tempting idea, if it works, might help us find out the optimal τ_l - τ_m combination, revealing a more realistic relationship between optical depths in different layers and the global irradiance.

Appendix A. Approaches for solving the RTE

A.1. Successive orders of scattering

By expressing the radiation as a series:

$$I^*(\tau, \mu, \theta) = \sum_{n=1}^{\infty} I_n^*(\tau, \mu, \theta), \quad (\text{A.1})$$

where $I_n^*(\tau, \mu, \theta)$ refers to the n th order of the scattering. As in Section 2.1, without azimuthal dependence, the primary scattering from the direct solar beam is found in Eq. (2.22):

$$S_1(\tau, \mu) = \frac{\tilde{\omega}(\tau)}{4\pi} Q_0^\downarrow P(\tau, \mu, -\mu_0) e^{-\frac{\tau}{\mu_0}}, \quad (\text{A.2})$$

when $n > 1$, we have:

$$S_n(\tau, \mu) = \frac{\tilde{\omega}(\tau)}{2} \int_{-1}^1 P(\tau, \mu, \mu') I_{n-1}(\tau, \mu') d\mu'. \quad (\text{A.3})$$

From Eq. (2.13), we can write:

$$I_n^*(\tau, \mu < 0) = -\frac{1}{\mu} \int_0^\tau S_n(\tau', \mu) e^{-\frac{\tau'-\tau}{\mu}} d\tau'. \quad (\text{A.4})$$

Upon substituting Eq. (A.2) into Eq. (A.4), letting $\tau = \tau_b$, we find the first order $n = 1$ of diffuse transmitted radiation to be:

$$I_1^*(\tau_b, \mu < 0) = \frac{\mu_0}{\mu_0 + \mu} \frac{Q_0^\downarrow \tilde{\omega}}{4\pi} \bar{P}(\mu, -\mu_0) \left(e^{-\frac{\tau_b}{\mu_0}} - e^{\frac{\tau_b}{\mu}} \right), \quad (\text{A.5})$$

where \bar{P} and $\tilde{\omega}$ respectively represents the average phase function and average single scattering albedo in the atmosphere with thickness τ_b . With Eqs. (A.2) and (A.5) as starting points, we can make use of Eqs. (A.3) and (A.4) to iteratively obtain each order's radiation caused by corresponding scattering events, and finally we add them up as in Eq. (A.1).

A.2. Invariant imbedding

Assuming an atmospheric layer with optical depth τ_b , where only diffuse shortwave radiation is concerned, the reflection function $\mathcal{R}(\tau_b, \mu, \theta, \mu', \theta')$, and the transmission function $\mathcal{T}(\tau_b, \mu, \theta, \mu', \theta')$ can be defined as (Liou 2002):

$$I^*(0, \mu > 0, \phi) = \frac{1}{\pi} \int_0^{2\pi} \int_0^1 \mathcal{R}(\tau_b, \mu, \phi, \mu', \phi') I(0, \mu' < 0, \phi') \mu' d\mu' d\phi', \quad (\text{A.6})$$

$$I^*(\tau_b, \mu < 0, \phi) = \frac{1}{\pi} \int_0^{2\pi} \int_0^1 \mathcal{T}(\tau_b, \mu, \phi, \mu', \phi') I(0, \mu' < 0, \phi') \mu' d\mu' d\phi'. \quad (\text{A.7})$$

Note that \mathcal{R} and \mathcal{T} are not functions of τ , but of τ_b . Substituting in Eq. (2.8) leads to:

$$\mathcal{R}(\tau_b, \mu, \phi, \mu', \phi') = \frac{\pi I^*(0, \mu > 0, \phi)}{\mu_0 Q_0^\downarrow}, \quad (\text{A.8})$$

$$\mathcal{T}(\tau_b, \mu, \phi, \mu', \phi') = \frac{\pi I^*(\tau_b, \mu < 0, \phi)}{\mu_0 Q_0^\downarrow}. \quad (\text{A.9})$$

By adding a thin layer above the TOA (here “thin” means that in such layer scattering more than once can be safely neglected), considering the change of \mathcal{R} and \mathcal{T} between the augmented atmosphere with “imbedded” layer and the original one, differential equations that do not involve the intensity I can be established, and, by neglecting the azimuthal dependence and temporarily the surface reflection, equations of \mathcal{R} and \mathcal{T} can be found in the form (Zdunkowski *et al.* 2007):

$$\begin{aligned} \frac{(\mu_0 + \mu) Q_0^\downarrow}{\pi} \mathcal{R}(\tau_0, \mu, \mu_0) &= 2\mu \int_0^1 \mathcal{R}(\tau_0, \mu, \mu') S(0, -\mu') d\mu' \\ &\quad - 2\mu \int_0^1 \mathcal{T}(\tau_0, \mu, \mu') S(\tau_b, \mu') d\mu' + S(0, \mu) - S(\tau_b, \mu) e^{-\frac{\tau_b}{\mu}}, \end{aligned} \quad (\text{A.10})$$

$$\begin{aligned} \frac{(\mu_0 + \mu) Q_0^\downarrow}{\pi} \mathcal{T}(\tau_0, \mu, \mu_0) &= 2\mu \int_0^1 \mathcal{R}(\tau_0, \mu, \mu') S(\tau_b, \mu') d\mu' \\ &\quad - 2\mu \int_0^1 \mathcal{T}(\tau_0, \mu, \mu') S(0, -\mu') d\mu' + S(\tau_b, -\mu) - S(0, -\mu) e^{-\frac{\tau_b}{\mu}}, \end{aligned} \quad (\text{A.11})$$

where source functions are:

$$S(0, \mu) = \frac{\tilde{\omega}}{2\pi} \mu Q_0^\downarrow \int_0^1 \mathcal{R}(\tau_0, \mu', \mu_0) P(\mu, \mu') d\mu' + \frac{\tilde{\omega}}{4\pi} Q_0^\downarrow P(\mu, -\mu_0), \quad (\text{A.12})$$

$$S(\tau_b, \mu) = \frac{\tilde{\omega}}{2\pi} \mu Q_0^\downarrow \int_0^1 \mathcal{T}(\tau_0, \mu', \mu_0) P(\mu, -\mu') d\mu' + \frac{\tilde{\omega}}{4\pi} Q_0^\downarrow e^{-\frac{\tau_b}{\mu_0}} P(\mu, -\mu_0). \quad (\text{A.13})$$

Further, \mathcal{R} and \mathcal{T} can be expressed by Chandrasekhar's X and Y functions:

$$X(\mu) = 1 + \mu \int_0^1 \frac{\Psi(\mu')}{\mu' + \mu} [X(\mu)X(\mu') - Y(\mu)Y(\mu')] d\mu', \quad (\text{A.14})$$

$$Y(\mu) = e^{-\frac{\tau_b}{\mu}} + \mu \int_0^1 \frac{\Psi(\mu')}{\mu' - \mu} [X(\mu)Y(\mu') - X(\mu')Y(\mu)] d\mu', \quad (\text{A.15})$$

where $\Psi(\mu)$ refers to the *characteristic function*. For the case of isotropic scattering, $\Psi(\mu) = \tilde{\omega}/2$, rather simple expressions for \mathcal{R} and \mathcal{T} can then be found:

$$\left(\frac{1}{\mu} + \frac{1}{\mu_0}\right) \mathcal{R}(\tau_b, \mu, \mu_0) = \frac{\tilde{\omega}}{4\mu\mu_0} [X(\mu)X(\mu_0) - Y(\mu)Y(\mu_0)], \quad (\text{A.16})$$

$$\left(\frac{1}{\mu} - \frac{1}{\mu_0}\right) \mathcal{T}(\tau_b, \mu, \mu_0) = \frac{\tilde{\omega}}{4\mu\mu_0} [X(\mu)Y(\mu_0) - X(\mu_0)Y(\mu)]. \quad (\text{A.17})$$

Numerical results of X and Y functions under isotropic scattering were tabulated by authors like Carlstedt and Mullikin (1966); Fuller and Hyett (1968), etc.

Finally, when a surface is non-black, with reflection terms to be added to Eqs. (A.8) and (A.9), the extra effort is not excessive (Liou 2002; Zdunkowski *et al.* 2007). In essence, mathematically speaking, invariant imbedding turns a two-point boundary-value problem into an initial value problem (Bellman and Wing 1992), and instead of coping with details within the medium, only emerging radiations from the two boundaries are need in calculations.

A.3. Adding and doubling

On the grounds of Eqs. (A.6) and (A.7), functions \mathcal{R} and \mathcal{T} can be utilized as operators, and by assuming an atmospheric layer (Layer 1) of optical depth τ_1 and ignoring emission, we can write (cf. Eq. (2.29)) (Goody and Yung 1995):

$$\begin{bmatrix} \mathbf{I}^\uparrow(0) \\ \mathbf{I}^\downarrow(\tau_1) \end{bmatrix} = \begin{bmatrix} \mathcal{R}_1 & \tilde{\mathcal{T}}_1 \\ \mathcal{T}_1 & \tilde{\mathcal{R}}_1 \end{bmatrix} \begin{bmatrix} \mathbf{I}^\downarrow(0) \\ \mathbf{I}^\uparrow(\tau_1) \end{bmatrix}, \quad (\text{A.18})$$

where \mathcal{R}_1 and \mathcal{T}_1 are matrix operators for downward radiation, while $\tilde{\mathcal{R}}_1$ and $\tilde{\mathcal{T}}_1$ are ones referring to upward radiation. Eq. (A.18) is known as the *interaction principle* (Grant and Hunt 1969). Like *invariant imbedding* in Appendix A.2, information inside the layer is not of interest, vector operators \mathcal{R} , \mathcal{T} can be obtained through applying the foregoing mentioned Gaussian quadrature (cf. Section 2.2.1) to Eqs. (A.6) and (A.7). By adding a layer (Layer 2) of thickness $\tau_2 - \tau_1$ below Layer 1, we likewise get a second matrix equation:

$$\begin{bmatrix} \mathbf{I}^\uparrow(\tau_1) \\ \mathbf{I}^\downarrow(\tau_2) \end{bmatrix} = \begin{bmatrix} \mathcal{R}_2 & \tilde{\mathcal{T}}_2 \\ \mathcal{T}_2 & \tilde{\mathcal{R}}_2 \end{bmatrix} \begin{bmatrix} \mathbf{I}^\downarrow(\tau_1) \\ \mathbf{I}^\uparrow(\tau_2) \end{bmatrix}. \quad (\text{A.19})$$

If we only care about reflection and transmission functions of the *combined* layer $0 \sim \tau_2$ (Layer 12), we can eliminate $\mathbf{I}^{\uparrow\downarrow}(\tau_1)$ in Eqs. (A.18) and (A.19), then obtain relationships of solely $\mathbf{I}^{\uparrow\downarrow}(0)$ and $\mathbf{I}^{\uparrow\downarrow}(\tau_2)$ for Layer 12:

$$\begin{bmatrix} \mathbf{I}^\uparrow(0) \\ \mathbf{I}^\downarrow(\tau_2) \end{bmatrix} = \begin{bmatrix} \mathcal{R}_{12} & \tilde{\mathcal{T}}_{12} \\ \mathcal{T}_{12} & \tilde{\mathcal{R}}_{12} \end{bmatrix} \begin{bmatrix} \mathbf{I}^\downarrow(0) \\ \mathbf{I}^\uparrow(\tau_2) \end{bmatrix}, \quad (\text{A.20})$$

where

$$\begin{bmatrix} \mathcal{R}_{12} & \tilde{\mathcal{T}}_{12} \\ \mathcal{T}_{12} & \tilde{\mathcal{R}}_{12} \end{bmatrix} = \begin{bmatrix} \mathcal{R}_1 + \tilde{\mathcal{T}}_1(\mathbf{1} - \mathcal{R}_2\tilde{\mathcal{R}}_1)^{-1}\mathcal{R}_2\mathcal{T}_1 & \tilde{\mathcal{T}}_1(\mathbf{1} - \mathcal{R}_2\tilde{\mathcal{R}}_1)^{-1}\tilde{\mathcal{T}}_2 \\ \mathcal{T}_2(\mathbf{1} - \tilde{\mathcal{R}}_1\mathcal{R}_2)^{-1}\mathcal{T}_1 & \tilde{\mathcal{R}}_2 + \mathcal{T}_2(\mathbf{1} - \tilde{\mathcal{R}}_1\mathcal{R}_2)^{-1}\tilde{\mathcal{R}}_1\tilde{\mathcal{T}}_2 \end{bmatrix}, \quad (\text{A.21})$$

here $\mathbf{1}$ denotes the identity matrix. Eq. (A.21) represents so-called *addition theorems*, from which we can obtain the combined layer's properties from properties of each independent layer.

If a layer is homogeneous, ignoring polarization and azimuthal dependence, then $\mathcal{R} = \tilde{\mathcal{R}}$ and $\mathcal{T} = \tilde{\mathcal{T}}$ (Hovenier 1969). Further, when the adding layer is optically identical as the original one, Eq. (A.21) becomes:

$$\begin{bmatrix} \mathcal{R}_{11} \\ \mathcal{T}_{11} \end{bmatrix} = \begin{bmatrix} \mathcal{R}_1 + \mathcal{T}_1(\mathbf{1} - \mathcal{R}_1^2)^{-1}\mathcal{R}_1\mathcal{T}_1 \\ \mathcal{T}_1(\mathbf{1} - \mathcal{R}_1^2)^{-1}\mathcal{T}_1 \end{bmatrix}. \quad (\text{A.22})$$

Eq. (A.22) is referred to as the *doubling* method. *Adding* and *doubling* can thus be elaborated in the following steps:

1. divide an inhomogeneous atmosphere into several fictitious layers, each layer regarded as vertically homogeneous.
2. further divide a homogeneous layer into 2^n “thin enough” sublayers, where the concept “thin” can be based on the same idea mentioned in Appendix A.2, so only the primary scattering takes place in such a sublayer, then the properties are much easier to handle.
3. obtain properties of a thin sublayer of thickness τ_1 , “double” n times to find \mathcal{R} and \mathcal{T} of the homogeneous layer that has thickness of $(2^n \cdot \tau_1)$ by Eq. (A.22). Likewise for the other homogeneous layers.
4. making use of Eq. (A.21), add each homogeneous layer together, to finally get \mathcal{R} and \mathcal{T} of the whole atmosphere.

Appendix B. Data validation methodology

Before data are put to use, their quality should be validated. In a validation procedure, if a record fails any test of validation procedures, it will be marked with a questionable flag. In this appendix, the validation methodology we used is discussed, mainly for irradiance data.

Borrowing the idea proposed by O'Brien and Keefer (1985) for hydrological gauging data, Meek and Hatfield (1994) developed a systematic method to validate meteorological variables from individual stations, their methodology contains three general types of test: 1) whether the value is within the physically permitted range; 2) whether the rate of change is within a reasonable range; 3) whether the rate of change is unreasonably small in a time span. For solar irradiation, Younes *et al.* (2005) borrowed the "Page model" (Page 1997), and proposed a more sophisticated empirical algorithm, which defines an envelope with upper and bottom boundary in calculating clearness index. Moradi (2009) also used a three-step test, but deciding the value range based on Ångström–Prescott equation.

B.1. Validation procedure

B.1.1. Irradiance data

Global irradiance dataset is tested by the seven steps shown below. The hourly irradiance record is denoted as Q_h .

Valid test The data logger might not be working appropriately all the time, missing data will be marked as "invalid".

Rigid Bound Test This step is to test whether the record is within a permitted range, assumed by Schuster (1905), $1500 W/m^2$, was used, but since the irradiation only fluctuates 6.9% around the solar constant in a year, from $1321 W/m^2$ to $1412 W/m^2$ (see Section 4.1), it should suffice to set the upper boundary at $1420 W/m^2$:

$$-10 < Q_h < 1420 W/m^2. \tag{B.1}$$

Note that the lower limit tolerance being set to -10 instead of 0 is based on the consideration that the pyranometer is not always perfectly calibrated, and a small negative overall shift has limited influence on daily calculation. Similarly hereinafter.

Dynamic bound test This step can be considered as a further and more meticulous step than the previous rigid bound test, where we take the extraterrestrial irradiation Q_0^\downarrow at any given moment into account.

$$(0.05 \cdot Q_0^\downarrow - 10) < Q_h < (Q_0^\downarrow + 10). \quad (\text{B.2})$$

If a record is too low (lower than $0.05 \cdot Q_0^\downarrow - 10$), we mark it as questionable. Considering cloud reflection and aerosol scattering from nocturnal man-made light source, the upper boundary is set to $Q_0^\downarrow + 10$, instead of Q_0^\downarrow . (Especially around the sunset time, there is more chance that recorded irradiance will exceed the extraterrestrial irradiance. This phenomenon was also noticed by Meek and Hatfield (1994), who proposed some possible explanations.)

Clear-sky bound test Many works (e.g., Moradi 2009, and Younes *et al.* 2005) test solar irradiation dataset by comparing records with presumed highest value that could be detected in the clear sky condition. Here a simple empirical equation is adopted, proposed by Allen (1996):

$$k_c = 0.75 + 2 \cdot 10^{-5} z, \quad (\text{B.3})$$

where z is the altitude of the concerned station. According to a suggestion by Allen (1996), this equation is suitable for altitudes from 0 m to 3000 m above sea level. Considering the elevation of Bogotá is very close to 3000 , we changed 0.75 to 0.80 , a more tolerant threshold.

Step test The step test compares the change between successive observations. If the difference exceeds an allowed value, the record will be marked. The step test has proven to be useful for detecting erroneous records due to loose wires or any other datalogger problems. We use a fixed rate-of-change limit, which follows the proposal by Shafer *et al.* (2000):

$$|Q_h - Q_{h-1}| \leq 800 \text{ W/m}^2. \quad (\text{B.4})$$

Persistence test The persistence test is designed to determine damaged instruments or “stuck” records (Shafer *et al.* 2000). It marks suspicious records that do not show any change over time (Meek and Hatfield 1994). We apply two substeps: first, the “simple persistence test”, to check the rule that consecutive three observations shouldn’t be exactly the same:

$$Q_h \neq Q_{h-1} \neq Q_{h-2}, \quad (\text{B.5})$$

Second, the “variance test”, to make sure the unbiased sample variance of 10 consecutive values should not be less than 0.1:

$$s^2 > 0.1[\text{for every 10 consecutive observations}]. \quad (\text{B.6})$$

B.1.2. Other variables

For other variables, the validation procedures are rather simple, physically unreasonable observations are discarded, normally only the rigid bound test is applied, e.g., for the surface temperature T , if a record is too high or too low (such as higher than 30°C or lower than 0°C), it will be marked.

B.2. Testing and preparing the dataset

We set the tolerance threshold as 1 in daytime, which means, if records in one day’s daytime (usually 13 hours) contain more than 1 marked records, the data from this day will not be used. Following this rule, combining validations of all variables, the station “EL IDEAM” has relatively plenty data left, with 1692 days’ records in ten years (from 2008 to 2017) that we picked out for numerical experiments.

Bibliography

- R. G. Allen. Assessing integrity of weather data for reference evapotranspiration estimation. *Journal of Irrigation and Drainage Engineering*, 122(2):97–106, 1996. ISSN 0733-9437.
- R. G. Allen. Self-calibrating method for estimating solar radiation from air temperature. *Journal of Hydrologic engineering*, 2:56–67, 1997. ISSN 1084-0699.
- V. Ambartsumian. Diffusion of light by planetary atmospheres. *Astron Zh*, 19:30–41, 1942.
- A. Ångström. Solar and terrestrial radiation. Report to the international commission for solar research on actinometric investigations of solar and atmospheric radiation. *Quarterly Journal of the Royal Meteorological Society*, 50:121–126, 1924. ISSN 1477-870X.
- A. Ångström. On the computation of global radiation from records of sunshine. *Arkiv Geof*, 2:471–479, 1956.
- J. Annandale, N. Jovanovic, N. Benade, and R. Allen. Software for missing data error analysis of Penman-Monteith reference evapotranspiration. *Irrigation Science*, 21(2):57–67, 2002.
- V. Bădescu. Observations concerning the empirical relationship of cloud shade to point cloudiness (Romania). *Journal of Applied Meteorology*, 29(12):1358–1360, 1990.
- V. Bădescu. Studies concerning the empirical relationship of cloud shade to point cloudiness (Romania). *Theoretical and applied climatology*, 44(3-4):187–200, 1991. ISSN 0177-798X.
- K. Bakirci. Correlations for estimation of solar radiation on horizontal surfaces. *Journal of Energy Engineering*, 134(4):130–134, 2008.
- K. Bakirci. Models of solar radiation with hours of bright sunshine: A review. *Renewable and Sustainable Energy Reviews*, 13(9):2580–2588, 2009.
- R. Bellman and R. Kalaba. On the fundamental equations of invariant imbedding, I. *Proceedings of the National Academy of Sciences*, 47(3):336–338, 1961.
- R. Bellman and G. M. Wing. *An Introduction to Invariant Imbedding*, volume 8. SIAM, 1992.

- F. Besharat, A. A. Dehghan, and A. R. Faghieh. Empirical models for estimating global solar radiation: A review and case study. *Renewable and Sustainable Energy Reviews*, 21: 798–821, 2013.
- M. Bevis, S. Businger, S. Chiswell, T. A. Herring, R. A. Anthes, C. Rocken, and R. H. Ware. GPS meteorology: Mapping zenith wet delays onto precipitable water. *Journal of Applied Meteorology*, 33(3):379–386, 1994. ISSN 1520-0450.
- A. J. Biga and R. Rosa. Estimating solar irradiation sums from sunshine and cloudiness observations. *Solar Energy*, 25:265–272, 1980. ISSN 0038-092X.
- R. E. Bird and C. Riordan. Simple solar spectral model for direct and diffuse irradiance on horizontal and tilted planes at the earth’s surface for cloudless atmospheres. *Journal of Climate and Applied meteorology*, 25:87–97, 1986. ISSN 0733-3021.
- K. L. Bristow and G. S. Campbell. On the relationship between incoming solar radiation and daily maximum and minimum temperature. *Agricultural and Forest Meteorology*, 31: 159–166, 1984. ISSN 0168-1923.
- W. Brutsaert. *Evaporation into the Atmosphere. Theory, History, and Applications*; Dordrecht: Holland, D. Reidel Co, 1982.
- I. W. Busbridge. *The Mathematics of Radiative Transfer*. University Press, 1960.
- J. Carlstedt and T. W. Mullikin. Chandrasekhar’s X-and Y-functions. *The Astrophysical Journal Supplement Series*, 12:449, 1966. ISSN 0067-0049.
- S. Chandrasekhar. *Radiative Transfer*. Oxford, 1950.
- S. Chandrasekhar. *Radiative Transfer*. Dover, Mineola, NY, 1960.
- R. Chen, K. Ersi, J. Yang, S. Lu, and W. Zhao. Validation of five global radiation models with measured daily data in China. *Energy Conversion and Management*, 45(11-12): 1759–1769, 2004.
- H. Cheyney III and A. Arking. A new formulation for anisotropic radiative transfer problems. I-Solution with a variational technique. *The Astrophysical Journal*, 207:808–819, 1976.
- F. Chollet. *Deep Learning with Python*. Manning Publications Co., 2017. ISBN 1-61729-443-8.
- J. A. Coakley Jr. and P. Chýlek. The two-stream approximation in radiative transfer: Including the angle of the incident radiation. *Journal of the Atmospheric Sciences*, 32(2): 409–418, 1975.

- R. E. Danielson, D. R. Moore, and H. C. Van de Hulst. The transfer of visible radiation through clouds. *Journal of the Atmospheric Sciences*, 26(5):1078–1087, 1969.
- M. Despotovic, V. Nedic, D. Despotovic, and S. Cvetanovic. Review and statistical analysis of different global solar radiation sunshine models. *Renewable and Sustainable Energy Reviews*, 52:1869–1880, 2015.
- H. L. Driedger and C. AJ. Estimation of solar radiation receipt from sunshine duration at Winnipeg. *Meteorological Magazine*, 99(1179):285–&, 1970.
- A. S. Eddington. *The Internal Constitution of the Stars*. Cambridge University Press, 1926. ISBN 978-0-521-33708-3.
- D. Elizondo, G. Hoogenboom, and R. W. McClendon. Development of a neural network model to predict daily solar radiation. *Agricultural and Forest Meteorology*, 71(1-2):115–132, 1994.
- H. K. Elminir, Y. A. Azzam, and F. I. Younes. Prediction of hourly and daily diffuse fraction using neural network, as compared to linear regression models. *Energy*, 32(8):1513–1523, 2007.
- P. Feautrier. Sur la resolution numerique de l’equation de transfert. *Comptes Rendus Académie des Sciences (série non spécifiée)*, 258, 1964.
- M. Frère. Estudio agroclimatológico de la zona andina: Informe técnico. Technical report, FAO/UNESCO, 1975.
- F. B. Fuller and B. J. Hyett. Calculations of Chandrasekhar’s X and Y functions and their analogs for noncoherent isotropic scattering. *NASA Technical note*, 1968.
- M. W. Gardner and S. R. Dorling. Artificial neural networks (the multilayer perceptron)—a review of applications in the atmospheric sciences. *Atmospheric environment*, 32(14-15): 2627–2636, 1998.
- J. Gariépy. Estimation of global solar radiation. *International Report, Service of Meteorology, Government of Quebec, Canada*, 1980.
- A. Géron. *Hands-on Machine Learning with Scikit-Learn and TensorFlow: Concepts, Tools, and Techniques to Build Intelligent Systems*. O’Reilly Media, Inc., 2017. ISBN 1-4919-6226-7.
- J. Glover and J. S. G. McCulloch. The empirical relation between solar radiation and hours of sunshine. *Quarterly Journal of the Royal Meteorological Society*, 84(360):172–175, 1958.
- R. M. Goody and Y. L. Yung. *Atmospheric Radiation: Theoretical Basis*. Oxford University Press, 1995. ISBN 0-19-535610-1.

- K. K. Gopinathan. A general formula for computing the coefficients of the correlation connecting global solar radiation to sunshine duration. *Solar energy*, 41(6):499–502, 1988.
- I. P. Grant and G. E. Hunt. Discrete space theory of radiative transfer I. Fundamentals. *Proc. R. Soc. Lond. A*, 313(1513):183–197, 1969.
- M. A. Guevara Luna, F. A. Guevara Luna, J. F. Méndez Espinosa, and L. C. Belalcázar Cerón. Spatial and Temporal Assessment of Particulate Matter Using AOD Data from MODIS and Surface Measurements in the Ambient Air of Colombia. *Asian Journal of Atmospheric Environment (AJAE)*, 12(2), 2018.
- C. Gueymard. Critical analysis and performance assessment of clear sky solar irradiance models using theoretical and measured data. *Solar Energy*, 51(2):121–138, 1993.
- C. A. Gueymard. Direct solar transmittance and irradiance predictions with broadband models. Part I: Detailed theoretical performance assessment. *Solar Energy*, 74(5):355–379, 2003a.
- C. A. Gueymard. Direct solar transmittance and irradiance predictions with broadband models. Part II: Validation with high-quality measurements. *Solar Energy*, 74(5):381–395, 2003b.
- M. T. Hagan, H. B. Demuth, and M. H. Beale. *Neural Network Design*. Martin Hagan, Sept. 2014. ISBN 978-0-9717321-1-7.
- G. H. Hargreaves and Z. A. Samani. Estimating potential evapotranspiration. *Journal of the Irrigation and Drainage Division*, 108(3):225–230, 1982.
- A. W. Harrison and C. A. Coombes. Empirical relationship of cloud shade to point cloudiness (Canada). *Solar Energy*, 37(6):417–421, 1986.
- L. G. Henyey and J. L. Greenstein. Diffuse radiation in the galaxy. *The Astrophysical Journal*, 93:70–83, 1941.
- J. W. Hovenier. Symmetry relationships for scattering of polarized light in a slab of randomly oriented particles. *Journal of the Atmospheric Sciences*, 26(3):488–499, 1969.
- D. V. Hoyt. Percent of possible sunshine and the total cloud cover. *Monthly Weather Review*, 105(5):648–652, 1977.
- L. A. Hunt, L. Kuchar, and C. J. Swanton. Estimation of solar radiation for use in crop modelling. *Agricultural and Forest Meteorology*, 91(3-4):293–300, 1998.
- M. Iqbal. *An Introduction to Solar Radiation*. Academic Press, Toronto; New York, 1983. ISBN 978-0-12-373752-6.

- Y. Jiang. Prediction of monthly mean daily diffuse solar radiation using artificial neural networks and comparison with other empirical models. *Energy Policy*, 36(10):3833–3837, 2008. ISSN 0301-4215.
- J. H. Joseph, W. J. Wiscombe, and J. A. Weinman. The delta-Eddington approximation for radiative flux transfer. *Journal of the Atmospheric Sciences*, 33(12):2452–2459, 1976.
- G. W. Kattawar, G. N. Plass, and J. A. Guinn Jr. Monte Carlo calculations of the polarization of radiation in the earth’s atmosphere-ocean system. *Journal of Physical Oceanography*, 3(4):353–372, 1973.
- T. Khatib, A. Mohamed, K. Sopian, and M. Mahmoud. Assessment of artificial neural networks for hourly solar radiation prediction. *International Journal of Photoenergy*, 2012, 2012. ISSN 1110-662X.
- H. H. Kimball. Variations in the total and luminous solar radiation with geographical position in the united states. *Monthly Weather Review*, 47(11):769–793, Nov. 1919. ISSN 0027-0644. doi: 10.1175/1520-0493(1919)47<769:VITTAL>2.0.CO;2.
- K. Y. Kondratyev. Radiation in the Atmosphere. *Radiation in the atmosphere., by Kondrat’ev, K. Ya.. New York, NY (USA): Academic Press, 915 p., 1969.*
- V. Kourganoff. *Basic Methods in Transfer Problems*. Oxford University Press, 1952.
- R. Kumar, R. K. Aggarwal, and J. D. Sharma. Comparison of regression and artificial neural network models for estimation of global solar radiations. *Renewable and Sustainable Energy Reviews*, 52:1294–1299, 2015. ISSN 1364-0321.
- B. Leckner. The spectral distribution of solar radiation at the earth’s surface—elements of a model. *Solar Energy*, 20:143–150, 1978. ISSN 0038-092X.
- G. Lewis. Estimates of irradiance over Zimbabwe. *Solar Energy*, 31(6):609–612, 1983.
- Z. Lin, N. Chen, Y. Fan, W. Li, K. Stamnes, and S. Stamnes. New treatment of strongly anisotropic scattering phase functions: The Delta-M+ method. *Journal of the Atmospheric Sciences*, 75(1):327–336, 2018.
- K.-N. Liou. A numerical experiment on Chandrasekhar’s discrete-ordinate method for radiative transfer: Applications to cloudy and hazy atmospheres. *Journal of the Atmospheric Sciences*, 30(7):1303–1326, 1973.
- K.-n. Liou. Analytic two-stream and four-stream solutions for radiative transfer. *Journal of the Atmospheric Sciences*, 31(5):1473–1475, 1974.
- K.-N. Liou. Applications of the discrete-ordinate method for radiative transfer to inhomogeneous aerosol atmospheres. *Journal of Geophysical Research*, 80(24):3434–3440, 1975.

- K.-N. Liou. *An Introduction to Atmospheric Radiation*, volume 84. Academic press, 2002. ISBN 0-08-049167-7.
- G. Lopez, F. J. Batlles, and J. Tovar-Pescador. Selection of input parameters to model direct solar irradiance by using artificial neural networks. *Energy*, 30(9):1675–1684, 2005.
- A. H. Maghrabi. Parameterization of a simple model to estimate monthly global solar radiation based on meteorological variables, and evaluation of existing solar radiation models for Tabouk, Saudi Arabia. *Energy conversion and management*, 50(11):2754–2760, 2009.
- R. Mahmood and K. G. Hubbard. Effect of time of temperature observation and estimation of daily solar radiation for the Northern Great Plains, USA. *Agronomy Journal*, 94(4):723–733, 2002.
- G. I. Marchuk, G. A. Mikhailov, R. A. Darbinjan, B. S. Elepov, M. A. Nazaraliev, and B. A. Kargin. *The Monte Carlo Methods in Atmospheric Optics*. Springer, 1980.
- J. A. Martínez-Lozano, F. Tena, J. E. Onrubia, and J. De La Rubia. The historical evolution of the Ångström formula and its modifications: Review and bibliography. *Agricultural and Forest Meteorology*, 33:109–128, 1984. ISSN 0168-1923.
- M. A. McEntee. A revision of the equation relating sunshine hours to radiation income for Ireland. *Irish Journal of Agricultural Research*, pages 119–125, 1980.
- B. H. McKellar and M. A. Box. The scaling group of the radiative transfer equation. *Journal of the Atmospheric Sciences*, 38(5):1063–1068, 1981.
- D. W. Meek and J. L. Hatfield. Data quality checking for single station meteorological databases. *Agricultural and Forest Meteorology*, 69(1-2):85–109, 1994.
- F. Meza and E. Varas. Estimation of mean monthly solar global radiation as a function of temperature. *Agricultural and Forest Meteorology*, 100(2-3):231–241, 2000.
- D. Mihalas. Stellar atmospheres. *San Francisco, WH Freeman and Co., 1978. 650 p.*, 1978.
- M. Mohandes, S. Rehman, and T. O. Halawani. Estimation of global solar radiation using artificial neural networks. *Renewable energy*, 14(1-4):179–184, 1998.
- I. Moradi. Quality control of global solar radiation using sunshine duration hours. *Energy*, 34(1):1–6, 2009.
- P. M. Morse and H. Feshbach. *Methods of Theoretical Physics. Part I*, volume 1. McGraw-Hill, 1953.

- T. Nakajima and M. Tanaka. Matrix formulations for the transfer of solar radiation in a plane-parallel scattering atmosphere. *Journal of Quantitative Spectroscopy and Radiative Transfer*, 35(1):13–21, 1986.
- F. Neuwirth. The estimation of global and sky radiation in Austria. *Solar Energy*, 24(5):421–426, 1980.
- K. J. O'Brien and T. N. Keefer. Real-time data verification. In *Computer Applications in Water Resources*, pages 764–770. ASCE, 1985.
- J. C. Ododo, A. T. Sulaiman, J. Aidan, M. M. Yuguda, and F. A. Ogbu. The importance of maximum air temperature in the parameterisation of solar radiation in Nigeria. *Renewable Energy*, 6(7):751–763, 1995.
- J. K. Page. Proposed quality control procedures for the meteorological office data tapes relating to global solar radiation, diffuse solar radiation, sunshine and cloud in the UK. *Report FCIBSE*, 1997.
- J. Pelkowski. El albedo terrestre. *Revista de la Academia Colombiana de Ciencias Exactas, Físicas y Naturales*, 31(121):499–520, 2007.
- J. Pelkowski. A physical rationale for generalized Ångström–Prescott regression. *Solar Energy*, 83(7):955–963, July 2009. ISSN 0038-092X. doi: 10.1016/j.solener.2008.12.011.
- G. W. Petty. *A First Course in Atmospheric Radiation*. Sundog Pub, 2006. ISBN 0-9729033-1-3.
- G. N. Plass and G. W. Kattawar. Reflection of light pulses from clouds. *Applied optics*, 10(10):2304–2310, 1971.
- J. A. Prescott. Evaporation from a water surface in relation to solar radiation. *Transactions of the Royal Society of South Australia*, 64(1):114–118, 1940.
- M. R. Rietveld. A new method for estimating the regression coefficients in the formula relating solar radiation to sunshine. *Agricultural Meteorology*, 19(2-3):243–252, 1978.
- S. Ruder. An overview of gradient descent optimization algorithms. *arXiv preprint arXiv:1609.04747*, 2016.
- C. Sagan and J. B. Pollack. Anisotropic nonconservative scattering and the clouds of Venus. *Journal of Geophysical Research*, 72(2):469–477, 1967.
- A. Schuster. Radiation through a foggy atmosphere. *The astrophysical journal*, 21:1, 1905. ISSN 0004-637X.

- K. Schwarzschild. Über das Gleichgewicht der Sonnenatmosphäre. *Nachrichten von der Gesellschaft der Wissenschaften zu Göttingen, Mathematisch-Physikalische Klasse*, 1906: 41–53, 1906.
- A. A. Sfeir. Solar radiation in Lebanon. *Solar Energy*, 26(6):497–502, 1981.
- M. A. Shafer, C. A. Fiebrich, D. S. Arndt, S. E. Fredrickson, and T. W. Hughes. Quality assurance procedures in the Oklahoma Mesonet. *Journal of Atmospheric and Oceanic Technology*, 17(4):474–494, 2000.
- V. V. Sobolev. *A Treatise on Radiative Transfer*. Perenos Luchistoĭ Énergii v Atmosferakh Zvezd i Planet. English. Van Nostrand, Princeton, N.J., 1963.
- J. W. Spencer. Fourier series representation of the position of the sun. *Search*, 2(5):172–172, 1971.
- K. Stamnes. The theory of multiple scattering of radiation in plane parallel atmospheres. *Reviews of Geophysics*, 24(2):299–310, 1986.
- K. Stamnes and P. Conklin. A new multi-layer discrete ordinate approach to radiative transfer in vertically inhomogeneous atmospheres. *Journal of Quantitative Spectroscopy and Radiative Transfer*, 31(3):273–282, 1984.
- K. Stamnes, S.-C. Tsay, W. Wiscombe, and K. Jayaweera. Numerically stable algorithm for discrete-ordinate-method radiative transfer in multiple scattering and emitting layered media. *Applied Optics*, 27(12):2502–2509, 1988.
- G. G. Stokes. IV. On the intensity of the light reflected from or transmitted through a pile of plates. *Proceedings of the Royal Society of London*, 11:545–556, 1862.
- R. K. Swartman and O. Ogunlade. Solar radiation estimates from common parameters. *Solar Energy*, 11(3-4):170–172, 1967.
- G. E. Thomas and K. Stamnes. *Radiative Transfer in the Atmosphere and Ocean*. Cambridge University Press, 2002. ISBN 0-521-89061-6.
- P. E. Thornton and S. W. Running. An improved algorithm for estimating incident daily solar radiation from measurements of temperature, humidity, and precipitation. *Agricultural and Forest Meteorology*, 93(4):211–228, 1999.
- I. T. Toğrul, H. Toğrul, and D. Evin. Estimation of global solar radiation under clear sky radiation in Turkey. *Renewable Energy*, 21(2):271–287, 2000.
- S. Twomey, H. Jacobowitz, and H. B. Howell. Matrix methods for multiple-scattering problems. *Journal of the Atmospheric Sciences*, 23(3):289–298, 1966.

- F. S. Tymvios, C. P. Jacovides, S. C. Michaelides, and C. Scouteli. Comparative study of Ångström's and artificial neural networks' methodologies in estimating global solar radiation. *Solar Energy*, 78(6):752–762, 2005. ISSN 0038-092X.
- H. C. Van de Hulst. Scattering in a Planetary Atmosphere. *The Astrophysical Journal*, 107:220, 1948. ISSN 0004-637X.
- H. C. Van de Hulst. *A New Look at Multiple Scattering*. NASA Institute for Space Studies, Goddard Space Flight Center, New York, N.Y., 1963. OCLC: 11743238.
- H. C. Van de Hulst. *Multiple Light Scattering: Tables, Formulas and Applications*. Academic Press, 1980. ISBN 0-12-710701-0.
- C. D. Whiteman and K. J. Allwine. Extraterrestrial solar radiation on inclined surfaces. *Environmental Software*, 1:164–169, 1986. ISSN 0266-9838.
- W. J. Wiscombe. The Delta–M method: Rapid yet accurate radiative flux calculations for strongly asymmetric phase functions. *Journal of the atmospheric sciences*, 34(9):1408–1422, 1977.
- W. J. Wiscombe and G. W. Grams. The backscattered fraction in two-stream approximations. *Journal of the Atmospheric Sciences*, 33(12):2440–2451, 1976.
- S. Younes, R. Claywell, and T. Muneer. Quality control of solar radiation data: Present status and proposed new approaches. *Energy*, 30(9):1533–1549, 2005.
- W. Zdunkowski, T. Trautmann, and A. Bott. *Radiation in the Atmosphere: A Course in Theoretical Meteorology*. Cambridge University Press, 2007. ISBN 1-139-46460-4.